Nanoparticle mediated CRISPR base editing rescues Kir7.1 function relevant to ocular channelopathy

Authors: Meha Kabra[1, 2, †], Pawan K. Shahi[1, 2, †], Yuyuan Wang[3, 4], Divya Sinha[2, 5], Allison Spillane[1], Gregory A. Newby[6, 7, 8], Shivani Saxena[2, 3, 4], Amr A. Abdeen[2, 3, 4], Kimberly L. Edwards[2, 5], Cole O. Theisen[2, 5], David M. Gamm[2, 9], David R. Liu[6, 7,8], Shaoqin Gong[2, 3, 4, 9], Krishanu Saha[1, 2, 3, 4, 10, *], Bikash R. Pattnaik[1,2,9, *]

Author affiliations: [1]Department of Pediatrics, University of Wisconsin-Madison, Madison, WI, United States. [2]McPherson Eye Research Institute, University of Wisconsin-Madison, Madison, WI, United States. [3]Department of Biomedical Engineering, University of Wisconsin-Madison, Madison, WI, United States. [4]Wisconsin Institute of Discovery, University of Wisconsin-Madison, Madison, WI, United States. [5]Waisman Center, University of Wisconsin-Madison, Madison, WI, United States. [6]Merkin Institute of Transformative Technologies in Healthcare, Broad Institute of Harvard and MIT, Cambridge, MA, United States. [7]Howard Hughes Medical Institute, Harvard University, Cambridge, MA, United States. [8]Department of Chemistry and Chemical Biology, Harvard University, Cambridge, MA, United States. [9]Department of Ophthalmology and Visual Sciences, University of Wisconsin-Madison, Madison, WI, United States. [10]Center for Human Genomics and Precision Medicine, University of Wisconsin-Madison, Madison, WI -, United States.

[†]**These authors contributed equally to this work.**

***Corresponding author: Email:** pattnaik@wisc.edu and ksaha@wisc.edu

Abstract
Leber Congenital Amaurosis (LCA16) is a progressive vision loss disorder caused by point mutations in the *KCNJ13* gene, which encodes an inward-rectifying potassium channel, Kir7.1. A nonsense mutation, W53X (c.158G>A), leads to premature truncation of the protein, which disrupts K^+ conductance and makes retinal pigmented epithelium (RPE) non-functional. While there are no current treatments for LCA16, here we explore CRISPR base editing as a strategy to correct the single base pair pathogenic variant. We show that silica nanoparticle (SNC)-mediated delivery of an adenine base editor (ABE8e) mRNA and single-guide RNA can precisely and efficiently correct the $KCNJ13^{W53X}$ mutation to restore Kir7.1 channel function in an induced pluripotent stem cell-derived RPE (iPSC-RPE) model of LCA16, as well as in patient-derived fibroblasts and in a new LCA16 mouse model. We observed a higher editing efficiency in LCA16 patient-derived fibroblasts (47.38% ± 1.02) than in iPSC-RPE (16.90% ± 1.58) with no detectable off-target editing. The restored channel function in the edited cells resulted in a phenotype comparable to wild-type cells, suggesting the possibility that this treatment could restore vision in LCA16 patients. Injection of ABE8e-carrying SNCs decorated with all-trans retinoic acid (ATRA) ligand into the subretinal space in LCA16 mice showed specific delivery only to RPE and resulted in gene correction in approximately 10% of RPE cells that received the editing machinery. We observed marginal recovery of electroretinogram (ERG) following correction of the W53X allele at the injection site with no further degeneration of RPE. These findings provide a foundation and a proof-of-concept to transition from bench to bedside and support its further development for treating pediatric blindness using a safer mode of SNC-mediated delivery of base editors.

Keywords: CRISPR, base editing, gene correction, *KCNJ13* loss-of-function nonsense mutation, Kir7.1 ion channel, Leber congenital amaurosis 16 (LCA16), inherited retinal blindness, induced pluripotent stem cells- retinal pigment epithelium (hiPSC-RPE).

Introduction

Leber congenital amaurosis (LCA16; OMIM#614186) is a severe form of autosomal recessive inherited retinal dystrophy (IRD) leading to progressive vision loss in early life. LCA16 is caused by loss of function of the Kir7.1 potassium ion channel (encoded by the *KCNJ13* gene, location#2q37.1, OMIM#603208) in the apical process of the retinal pigmented epithelium (RPE) cells of the eye(*1, 2*). The Kir7.1 channel controls K^+ homeostasis in the subretinal space to support phototransduction, phagocytosis, and signaling by the RPE. Several missense and nonsense loss-of-function mutations have been reported in *KCNJ13*, leading to diminished K+ conductance and altered electroretinogram (ERG) of the RPE (*3-10*).

There is no available therapy for LCA16 patients, and no mouse model with biallelic mutations in *KCNJ13* exists in which to test possible therapeutic strategies. Induced pluripotent stem cells from a patient with the homozygous W53X mutation in *KCNJ13* have been used to derive RPE cells (LCA16 iPSC-RPE) as a model to test potential treatments like translational readthrough inducing drugs (TRIDs) and AAV-mediated gene augmentation (*11*). However, TRIDs are known to have proteome-wide effects, and gene augmentation approaches suffer from immunogenicity concerns and may not provide long-term benefit. CRISPR gene editing, in principle, could correct the endogenous gene and permanently reverse the underlying cause of disease. This approach has been set forth to elicit therapeutic benefits in IRDs (*12*). However, this strategy would require precise correction of a single nucleotide, which is difficult to achieve in post-mitotic cells using CRISPR-Cas9 nucleases followed by either homology-directed repair (HDR) or non-homologous end joining (NHEJ) (*13-15*). Moreover, double-strand DNA break (DSB) formation at the target site would pose a significant risk of uncontrolled indels as well as other undesired cellular consequences like chromosomal translocations, large deletions, aneuploidy, p53 activation, chromothripsis, transposon insertions (*16-25*). Base editing, on the other hand, is poised to overcome these limitations by capitalizing on the RNA-guided programmability of CRISPR-Cas9 to deliver a base modification enzyme that can site-specifically convert a single nucleotide to another (*26*).

Most base editors use a Cas9 nickase fused to an engineered or evolved deaminase enzyme. Adenine base editors (ABEs) install A>G changes, while cytosine base editors (CBEs) install C>T changes within a small editing window specified by the single guide RNA (sgRNAs) (*27*). Base editing does not rely on HDR and therefore tends to be more efficient in non-dividing cells. While delivery of the larger base editor effectors can be challenging, silica nanoparticles (SNCs) provide significant advantages over viral vectors in that they can transiently and cell-specifically deliver many types of payloads including nucleic acids and proteins without integrating into the genome (*28-30*). It was recently reported that SNCs decorated with all-*trans*-retinoic acid (ATRA) can achieve tissue-specific delivery to RPE cells via subretinal injection providing an unrealized opportunity to explore SNC-mediated base editor delivery for precise gene correction in LCA16 (*31*).

Here, we explored the ability of SNC-delivered base editor to correct the endogenous pathogenic W53X *KCNJ13* point mutation and restore Kir7.1 channel function in cell lines, patient iPSC-derived RPE, and via subretinal injection in a new LCA16 mouse model that we engineered. ABE significantly outperformed a CRISPR-Cas9 HDR strategy in terms of efficiency and editing precision, and we found that SNC-mediated delivery was sufficient to achieve ~10% editing of RPE cells in the mouse retina – a level that is estimated to provide significant phenotypic rescue based on previous studies. Moreover, the high efficiency of - editing of patient-derived iPSC-RPE suggests the opportunity to pursue autologous cell therapies using engraftment of edited cells. Our work provides important proof-of-concept that base editing via SNC delivery is a viable strategy to tackle inherited retinal diseases like LCA16.

Methods

1. **Ethical guidance and animal protocols**

   All work with LCA16 patient-derived cells (fibroblasts, iPSCs, and iPSC-RPE) was carried out following institutional, national, and international guidelines and approved by the University of Wisconsin-Madison's institutional review board and Stem Cell Research Oversight Committee. The animal protocols were in accordance with the ARVO Statement for use in ophthalmic and vision science research and approved by the University of Wisconsin School of Medicine and Public Health Animal Care and Use Committee (ACUC).

2. **HEK Flp-In™ 293 stable cells with GFP tagged WT and W53X Kir7.1 expression**

   HEK Flp-In™ 293 host cells (ThermoFisher Scientific#R75007, MA), generated using a pFRT/lacZeo target site vector, were used to express GFP-tagged Kir7.1 (WT and W53X). These cells contain a single Flp Recombination Target (FRT) site at a transcriptionally active genomic locus to allow stable integration of GFP-tagged human *KCNJ13* sequence (WT and W53X). As these cells express the Zeocin™ gene under SV40 early promoter, a complete D-MEM high glucose media [10% FBS, 1% Pen-Strep, 2mM L-glutamine] containing 100 µg/ml Zeocin™ was used for maintenance. GFP-WT or GFP-W53X *hKCNJ13* gene sequence was integrated into the genome of these cells based on the manufacturer's guidelines. Briefly, the cells were co-transfected with FLP-In™ expression vector (pcDNA5/FRT) containing GFP-tagged *hKCNJ13* sequence (WT or W53X) created by in-fusion cloning, and pOG44 recombinase expression plasmid. The pOG44 plasmid with constitutive expression of the Flp recombinase under CMV promoter mediates the homologous recombination between the FRT sites of host cells and the expression vector such that the construct from the vector is inserted into the genome at the FRT site. This insertion brings the Hygromycin B resistance gene into frame, inactivates the zeocin fusion gene, and expresses the gene of interest under the CMV promoter. 48 hours post-co-transfection, the cells were passaged at 25% confluency to select stable transfectants in 200 µg/ml of Hygromycin B. The Hygromycin B resistant cell clones (n=15-20) were picked, maintained in 100 µg/ml Hygromycin B, and further expanded for their characterization by genotyping (Sanger sequencing) and protein expression (immunocytochemistry). The primers used for in-fusion cloning and Sanger sequencing are listed in Supplementary Table 1.

3. **Patient-derived fibroblasts and iPSC-RPE cell culture and maintenance**

   Fibroblasts derived from skin biopsy of an LCA16 patient (*7, 11*) with homozygous W53X mutation in *KCNJ13* were cultured and maintained in complete DMEM high glucose media containing 10% FBS and 1% Pen-Strep at 37 °C with 5% CO_2. Induced pluripotent stem cells (iPSCs), reprogrammed from patient-derived fibroblasts, were cultured on Matrigel and differentiated to iPSC-RPE using an approach similar to that previously described (Shahi et al. AJHG 2019; Sinha et al., AJHG 2020). Briefly, on D0 of differentiation, iPSCs were lifted using ReLeSR (Stem Cell Technologies; Cat# 05872) to generate embryoid bodies (EBs). The EBs were maintained overnight in mTeSR+ containing 10 µM ROCK inhibitor (R&D Systems; Cat# Y-27632). Then, over the next three days, the EBs were gradually transitioned to Neural Induction Media (NIM; DMEM: F12 1:1, 1% N2 supplement, 1x MEM nonessential amino acids (MEM NEAA), 1x GlutaMAX, and 2 µg/ml heparin (Sigma)). On D7, EBs were plated on Nunc 6-well plates coated with Laminin (ThermoFisher Scientific; Cat# 23017015; diluted 1:20 in DMEM/F12), and on D16, neurospheres were mechanically lifted. Remaining adherent cells were transitioned to retinal differentiation media (RDM; DMEM/F12 (3:1), 2% B27 without retinoic acid, 1% antibiotic-antimycotic solution) and allowed to differentiate to RPE. For the first four media changes, RDM was supplemented with 10 µM SU5402 (Sigma-Aldrich; Cat# SML0443-5MG) and 3 µM CHIR99021 (BioGems; Cat# 2520691). After >60 days of differentiation, iPSC-RPE cells were purified as described by Sharma et al. and cultured on desired surface (*32*). Briefly, cultures with differentiated patches of iPSC-RPE were dissociated using 1X TrypLE Select Enzyme (ThermoFisher; Cat# 12563011) and enriched for iPSC-RPE via magnetic activated cell sorting using anti-CD24 and anti-CD56 antibodies (Miltenyi Biotec). iPSC-RPE cells in the negative cell fraction were seeded on desired surface pre-coated with Laminin (ThermoFisher Scientific; Cat# 23017015; diluted 1:20 in DMEM/F12) and cultured.

4. **Silica-nanoparticles (SNCs) for adenine base editing and CRISPR-Cas9 gene editing**

We recently reported a safe and efficient nanoplatform, SNC, to deliver CRISPR gene editing and base editing components (*31*). SNCs were synthesized using a water-in-oil microemulsion method. The oil phase (1 ml) was prepared by mixing Triton X-100 (885 μL) with hexanol (0.9 mL) and cyclohexane (3.75 mL). An aliquot of aqueous solution (25 μL) containing the desired payload (ssODN or base editor mRNA + sgRNA, with a total nucleic acid concentration of 2 mg/mL) was mixed with the silica reagents: TEOS (4 μL), BTPD (6 μL) and N-(3-(triethoxysilyl) propyl)-1H-imidazole-4-carboxamide (TESPIC, 1 mg). The synthesis of TESPIC was reported previously (*31*). This mixture was homogenized by pipetting and then added to the oil phase (1 mL). The water-in-oil microemulsion was formed by vortexing for 1 min. Under vigorous stirring (1,500 rpm), an aliquot of 30% aqueous ammonia solution (4 μL) was added, and the water-in-oil microemulsion was stirred at 4 ^{o}C for 12 h to obtain unmodified SNCs. Acetone (1.5 mL) was added to the microemulsion to precipitate the SNCs. The precipitate was recovered by centrifugation and washed twice with ethanol and three times with ultrapure water. The purified SNCs were collected by centrifugation. The as-prepared, unmodified SNC was re-dispersed in ultrapure water (1 mL). For surface modification, mPEG-silane or a mixture of mPEG-silane + silane-PEG-NH_2 (molar ratio of mPEG-silane: silane-PEG-NH_2 = 8:2) was added to the above-mentioned SNC suspension, for the synthesis of SNC-PEG without ATRA (i.e., SNC-PEG) or SNC-PEG-NH_2 (for ATRA conjugation), respectively. The total amount of PEG is 10 wt% of SNC. The pH of the suspension was adjusted to 8.0 using a 30% aqueous ammonia solution. The mixture was stirred at room temperature for 4 h. The resulting SNCs were purified by washing with ultrapure water three times and concentrated with Amicon® Ultra Centrifugal Filters (Millipore Sigma, USA). ATRA was conjugated onto SNC-PEG-NH_2 via EDC/NHS catalyzed amidation. Payload-encapsulated SNC-PEG-NH_2 (0.5 mg) was re-dispersed in 1 mL DI water. EDC (7.5 μg), NHS (4.5 μg), and a DMSO solution of ATRA (6 μg in 5 μL DMSO) were added to the above solution. The solution was stirred at room temperature for 6 h, and then the resulting ATRA-conjugated SNC (i.e., SNC-PEG-ATRA) was washed with water three times. The SNC-PEG-ATRA was concentrated with Amicon Ultra Centrifugal Filters to a payload concentration of 2 mg/ml before use. **Materials:** Tetraethyl orthosilicate (TEOS), Triton X-100, acetone, ethanol, 1-ethyl-3-(3-dimethylaminopropyl)carbodiimide (EDC), N-hydroxysuccinimide (NHS), and ammonia (30% water) were purchased from Fisher Scientific, USA. Hexanol and cyclohexane were purchased from Tokyo Chemical Industry Co., Ltd., USA. Dimethyl sulfoxide (DMSO) was purchased from Alfa Aesar, USA. Bis[3-(triethoxysilyl)propyl]-disulfide (BTPD) was purchased from Gelest, Inc., USA. Methoxy-poly (ethylene glycol)-silane (mPEG-silane, Mn = 5000) and amine-poly (ethylene glycol)-silane (NH2-PEG-silane, Mn = 5000) were purchased from Biochempeg Scientific Inc., USA. All-trans-retinoic acid (ATRA) was purchased from Santa Cruz Biotechnology, USA.

5. **Base editor mRNAs**

Using their mammalian-optimized UTR sequences, base editor mRNA was obtained as a custom product from Trilink Biotechnologies. The mRNAs were synthesized with complete substitution of uracil by N1-methylpseudouridine, co-transcriptional 5' capping with the CleanCap AG analog resulting in a 5' Cap1 structure, and included a 120 nucleotide polyA tail.

6. **sgRNA design**

The sgRNAs targeting W53X location in human *KCNJ13* gene was designed using Benchling (https://www.benchling.com). The design was also validated with two other online tools, CRISPR-RGEN (*33*) and PnB Designer (*34*), to confirm its on-target specificity (Supplementary Table 7). Only one sgRNA [Fig 2C] appeared to be very specific for the W53X location as it would allow the binding of the spCas9 domain to the target locus that positions c.158G>A site within the editing window of ABE (4-8 for ABE8e, counting the PAM as 21-23). This sgRNA also had the highest on-target score (65.7) and lowest off-target score (56.8) among the Benchling designed sgRNAs. The sgRNA targeting mouse *Kcnj13* was also selected based on the above criteria (highest on target score; 57.1, lowest off-target score; 56.8). The chemically modified form of these sgRNAs (human; G*C*G*CUAGCGUUGGAUGAUGU and mouse; G*C*G*CUAGCGCUGGAUGAUGC) were ordered from Synthego (CA, USA).

7. **Generation of the lentiviral vector for Cas9-mediated gene editing**
Lentivirus was manufactured for Cas9-mediated editing as described in Gándara, Carolina et al. (2018). Briefly, the HEK293 cells were plated and ready for transfection after 24□h after plating. Target plasmid was transfected to the HEK293 cells at 70% confluence, along with packaging gene plasmids pMD2.G and psPAX2. The target vector plasmid contains a copy of the LCAguide, Cas9 protein and mcherry reporter transgene driven by the EF□1α promoter. Cell culture supernatant was collected from HEK293 after transfection and was concentrated via gradient and centrifugation. A functional titer was performed to check the concentrated yield, between 10^7 and 10^{10} particles/mL.
8. **Gene editing in iPSC-RPE by lentiviral transduction (Cas9 and sgRNA delivery) and SNC (ssODN delivery)**
For our attempt to edit the *KCNJ13* gene carrying a W53X nonsense mutation, we used viral transduction to deliver Cas9 and an sgRNA (TAATGGACATGCGCTAGCGT) to the mature iPSC-RPE cells. We used lentiviral vectors (100 MOI) specifically designed for this purpose: lentiCRISPR v2-mCherry (Addgene plasmid # 99154), a gift from Agata Smogorzewska, with the annealed sgRNA oligonucleotides cloned into it using the BsmB1 enzyme digestion and ligation. Successful integration of the sgRNA sequence was confirmed by DNA sequencing with the primer 5′-GGACTATCATATGCTTACCG-3′ for the U6 promoter, which also drives sgRNA expression. Lentivirus was generated in-house using the method described above. This lentivirus was used to transduce mature iPSC-RPE cells to express Cas9, sgRNA, and the reporter gene mCherry, allowing easy identification of transduced cells. After 6 hours of viral transduction, 3 ug of the HDR repair template for W53X gene correction, ssODN-ATTO488 (GATGCTTGGGG**G**ATCCTAATGGA**T**ATGCGCT**G**GCGTTGGATGATGTT**A**GTCTTTTCTGCTTC T, the bold letters show the wobble changes), was delivered to the cells using SNC and incubated for 48 hours. Papain digestion was used to dissociate cells that expressed both red and green fluorescent markers, indicating that they had received both Cas9+sgRNA and ssODN constructs, into a single cell that was then used for patch-clamp experiments.
9. **Base editing in Kir7.1-HEK293 stable cells by electroporation**
HEK293 stable cells expressing $KCNJ13^{W53X}$-GFP were subcultured 24 hours prior to nucleofection at 70% confluency. The ABE8e mRNA (spCas9-NG, 3 µg) (*35*) and sgRNA (100 pmol) or ribonucleoprotein (RNP) complex formed by incubating the mixture of ABE8e protein (3 µg) and sgRNA (100 pmol) at room-temperature for 10 mins were introduced via electroporation. $1x10^5$ cells were electroporated using the FS-100 program in the Lonza 4D nucleofector according to the manufacturer's guidelines. Post-electroporation, cells were seeded in a 6-well plate and maintained in complete D-MEM media containing 100 µg/ml Hygromycin B for further analysis.
10. **Base editing in LCA16-patient's specific fibroblasts and iPSC-RPE by SNCs**
The W53X-LCA16-patient's specific fibroblasts ($Fibro^{W53X}$) were sub-cultured one day before treatment. For base editing, ABE8e mRNA (3 µg) and sgRNA (100 pmol) were delivered to fibroblasts using SNCs. 5 days post-treatment, DNA was isolated for genomic analysis. For base editing in iPSC-RPE, the cells were first seeded in a 96-well plate at a density of 50,000 cells per well in RDM containing 10% FBS and 10 µM ROCK inhibitor (R&D Systems; Cat# Y-27632). On Day 2, the media was switched to RDM containing 2% FBS. On day 3 post-seeding, ABE8e mRNA (3 µg) and sgRNA (100 pmol) were delivered to the cells using SNCs in RDM. the iPSC-RPE monolayer was dissociated 2 days post-treatment with SNC-ABE. Cells were seeded on transwell inserts and also collected for genomic DNA analysis. iPSC-RPE cells transitioned to transwell inserts were cultured for 4-6 weeks to get a polarized monolayer of RPE and subsequently analyzed for Kir7.1 channel function by whole-cell patch-clamp approach. Untreated cells were used as references.
11. **Base editing in mice**
C57BL/6J male and female mice ($Kcnj13^{+/+}$, $Kcnj13^{W53X/+}$) were housed at the animal facility at UW Madison (Madison, WI) under a 12-hour light-dark cycle at a controlled temperature (25±5 °C) and humidity (40–50%). The mice were genotyped using standard PCR methods with the primers listed in Supplementary Table 2, followed by digestion with restriction enzyme NheI (Anza# IVGN0066,

ThermoFisher). The W53X mutation creates a restriction site for NheI, and therefore the W53X allele resulted in two (212 bp and 302 bp) fragments compared to only one (514 bp) fragment in the WT allele (Supplementary figure 1). As homozygous W53X mice (*Kcnj13*$^{W53X/W53X}$) do not survive, we specifically knocked down the WT-*Kcnj13* allele using CRISPR-Cas9 in the eyes of *Kcnj13*$^{W53X/+}$ (n=3) to silence Kir7.1 expression. ERG (detailed method below, section 17) was conducted to confirm the loss of function, and the mice (*Kcnj13*$^{W53X/-}$) with reduced or no c-wave was used for the base editing of the W53X-*Kcnj13* allele. A subretinal injection (2 µl) of SNC-PEG-ATRA encapsulating ABE8e mRNA (3 µg), W53X-targeting sgRNA (100 pmol), and GFP mRNA (1 µg, to visualize the site of injection) was performed in mice (n=4 eyes). PBS or empty SNC-PEG-ATRA (n=4) injected eyes were used as reference. 5 days post-injection, DNA was isolated from the optic cup of these mice for genomic analysis.

12. On-target analysis by deep sequencing

Treated and untreated cells were dissociated using enzymatic treatment (Accutase/Papain) according to manufacturer's instructions for genomic analysis. From the HEK293 stable cells, total RNA (Qiagen#74134) was isolated, and reverse transcribed to cDNA (ThermoFisher#4368814), and subsequently amplified for on-target analysis using *KCNJ13* Illumina-specific primers (Supplementary Table 3). From fibroblasts, iPSC-RPE, and mouse optic cup, genomic DNA was isolated according to manufacturer's guidelines (Quick-DNA™ Miniprep plus kit #D4069) and quantified using Nanodrop 2000 or Qubit (Thermo Fisher). For deep sequencing of the *KCNJ13* locus, genomic DNA was amplified using Illumina specific primers with adapter sequences (amplicon size ~150 bp) (Supplementary Table 3). Unique indexes (i7 and i5) were ligated to each custom amplicon by PCR (amplicon size 250 bp), and the indexed amplicons were pooled and purified using AMPure XP beads (Beckman Coulter #A63881). The indexed library was run on an Illumina MiniSeq instrument, with a read length of 150bp. Deep sequencing data were analyzed using RGEN Cas-analyzer (*36*) (http://www.rgenome.net/cas-analyzer/) and CRISPResso2 (*37*) (https://crispresso.pinellolab.partners.org/submission) software.

13. Off-target analysis by deep sequencing

The potential off-target sites for the hW53X-sgRNA were identified by an in-silico tool, Cas-OFFinder (*38*) (http://www.rgenome.net/cas-offinder/). The parameters used were an NG/NGG/NAG PAM, and with up to 4 mismatches to the sgRNA sequence (Supplementary Table 4, Supplementary Figure 1). We also considered a DNA and RNA bulge of 1 nucleotide which occurs due to an extra unpaired base in the DNA sequence with respect to sgRNA or an extra unpaired base in sgRNA for DNA sequence in the genome respectively. From the treated and untreated stable cells, fibroblasts and iPSC-RPE, gDNA was isolated and amplified using primers specific to off-target sites. All the primer sequences are listed in Supplementary Table 5. The deep sequencing and data analysis were performed as mentioned above.

14. rhAmp off-target analysis in W53X mice

As the genomic DNA yield from the mouse optic cup was too low to amplify all the off-target sites separately, we used a highly efficient RNase H2-dependent (rhAmp) PCR technique that can amplify different targets in a single PCR reaction. Amplification and sequencing were performed according to IDT's rhAmp manual instructions). Briefly, the rhAmpSeq CRISPR panel was designed using the IDT-designing tool (https://www.idtdna.com/pages/tools/rhampseq-design-tool)for the potential off-targets of mW53X-sgRNA identified using Cas-OFFinder (Supplementary Table 6). The amplicon library was prepared using rhAmpSeq CRISPR Library Kit (IDT#10007317) and rhAmpSeq i5 and i7 index primers. The purified library was sequenced on the miniseq instrument from illumina. Sequencing analysis was performed using IDT-rhAMP CRISPR analysis tool (https://www.idtdna.com/site/analysislab).

15. Immunocytochemistry

Kir7.1 protein expression was assessed in the pool of W53X-mutant, WT, and base edited HEK293 stable cells by immunocytochemistry as described earlier (*10*). As the protein is GFP tagged, GFP mouse monoclonal primary antibody (Cell Signaling#2955, 1:250) was used to enhance the Kir7.1 protein expression for its detection in the cells. Sodium Potassium ATPase rabbit monoclonal primary antibody (Thermo Fisher#ST0533, 1:500) was used to label the cell membranes. Alexa fluor-594 conjugated Donkey anti-Rabbit (Proteintech#SA00006.8, 1:500) and Alexa fluor-488 conjugated Donkey anti-Mouse

(Proteintech#SA00006.5, 1:500) secondary antibodies were used. DAPI was used as a nuclear counterstain. Immunostained cells were imaged on a confocal microscope (Nikon C2 Instrument).

16. Electrophysiology assay

A high throughput automated patch clamp (Q Patch II, Sophion, Denmark) was used to measure the whole-cell current from the HEK^{WT}, $HEK^{W53X,}$ and base edited HEK^{W53X} stable cells as described earlier (*39*). Briefly, the cells were grown in a T75 flask for 48-72 hours and then detached gently using Detachin^{TM}. The cells were centrifuged at 90 x g for 1 min and resuspended in serum-free media containing 25 mM HEPES. The cells [3 M/ml] were kept on a shaker for 20 mins before the experiment. 48 cells were recorded in parallel on single-hole disposable Qplates with individual amplifiers. A pressure protocol was used to achieve cell positioning (-70 mbar), Giga seal (-75 mbar), and whole-cell configuration (5 pulses with -50 mbar increment between the pulses, first pulse of -250 mbar). The current was recorded in response to voltage-clamp steps from the holding potential (-10mV) to voltages between -140mV and +40mV (Δ=10mV). More than 70% of the cells completed the experiment. The cells in which the stability was compromised during the experiment were judged by the leak current and excluded from the analysis. The extracellular solution contained (in mM): 135 NaCl, 5 KCl, 10 HEPES, 10 glucose, 1.8 $CaCl_{2,}$ and 1 $MgCl_{2,}$ pH adjusted to 7.4 and osmolarity 305 mOsm. The intracellular solution contained (in mM) 30 KCl, 83 K-gluconate, 10 HEPES, 5.5 EGTA, 0.5 $CaCl_2$, 4 Mg-ATP, and 0.1 GTP, pH adjusted to 7.2 and osmolarity 280 mOsm. In an alternative external solution, NaCl was replaced with RbCl [140 mM] and used as an enhancer of Kir7.1 current. Extracellular solution with 20 mM Cs^+ was used to block Kir7.1 current. The data was analyzed using Sophion Analyzer v6.6.44. Whole-cell manual patch-clamp recording of base edited hiPS-RPE cells was performed according to the standard protocol described elsewhere (*7*).

17. Electroretinography (ERG) in mice

ERG was performed in mice using a standard protocol described elsewhere (*40*), before and after the base editing to evaluate the function of the retina. Briefly, the mice were dark-adapted overnight prior to ERG. ERG signals were captured in full darkness using an Espion Ganzfeld full-field system (Diagnosys LLC, Lowell, MA). When using a contact electrode, a drop of 2% hypromellose solution was applied to the eye in order to keep the cornea wet and make an electrical contact. For a and b-wave, the eyes were exposed to a series of flash intensities (0.03 to 30 cd.s/m2) using ganzfeld dome for 400 ms with a 2 s interval between each flash. For c-wave, the eyes were exposed to 25 cd.s/m2 for 4 s. Animals were subjected to ERG every 2 weeks, and data acquired were analyzed with Espion software (Diagnosys LLC, Lowell, Massachusetts) and Origin2018b OriginLab Corp., MA).

18. Statistical analysis

The data analysis was done using Origin software (Origin 2020, OriginLab Corporation, Northampton, MA, USA) and expressed as mean ± standard error. Two-tailed unpaired Student's *t*-test was used to determine the statistical differences, and $p < 0.05$ was considered significant.

Results

1. Low efficiency CRISPR-Cas9 nuclease repair of W53X mutation in patient iPSC-RPE^{W53X}

We first assessed the correction of the *KCNJ13* W53X mutation in iPSC-derived RPE (iPSC-RPE^{W53X}) using Cas9 nuclease-mediated HDR. We delivered Cas9 nuclease and sgRNA via the lentiviral vector LentiCRISPRv2-mCherry (Supplementary Figure 3), and the HDR donor template via silica-nanoparticle (SNC), and confirmed delivery of both constructs using their cognate fluorescent reporters [Fig 1A]. Deep sequencing analysis of the treated samples indicated that most of the indels (5.05 ± 1.24%) were created downstream of the pathogenic mutation (TAG), resulting in no change to the reading frame [Fig 1B-C]. Only a small fraction of reads showed in-frame indel formation (1.03 ± 0.52%) and WT genotype (0.34%) [Fig 1D]. Although the green fluorescence in the treated cells showed a successful delivery of ssODN, we did not observe the inclusion of any silent nucleotide bases from the ssODN [Fig 1B]. Most of the reads (94.50 ± 1.25%) were unedited in the treated cells.

Next, we measured Kir7.1 channel function in sorted populations of cells expressing the mCherry and GFP markers, indicating that they had received both Cas9-sgRNA and ssODN. Patch-clamp recordings revealed a normal Kir7.1 current with the inward current of -101.1 ± 35.54 pA at -150 mV in treated cells. Substitution of Na^+ with rubidium (Rb^+), a known activator of Kir7.1, increased the Kir7.1 inward current by 7-fold to -713.5 ± 92.97 pA [Fig 1E-G]. While these results suggest that acquisition of both Cas9-sgRNA and ssODN were conducive to function-restoring gene edits in some cases, this pooled assay obscures the exact nature and frequency of editing outcomes in the cells we measured, which was quantified based on the silent changes introduced by the ssODN.

Altogether, while this nuclease-mediated HDR approach did result in some functional rescue among edited cells – indicating that gene correction is a viable strategy to rescue Kir7.1 function in RPE cells – the low efficiency and imprecise nature of the edits diminished the translational potential of this strategy.

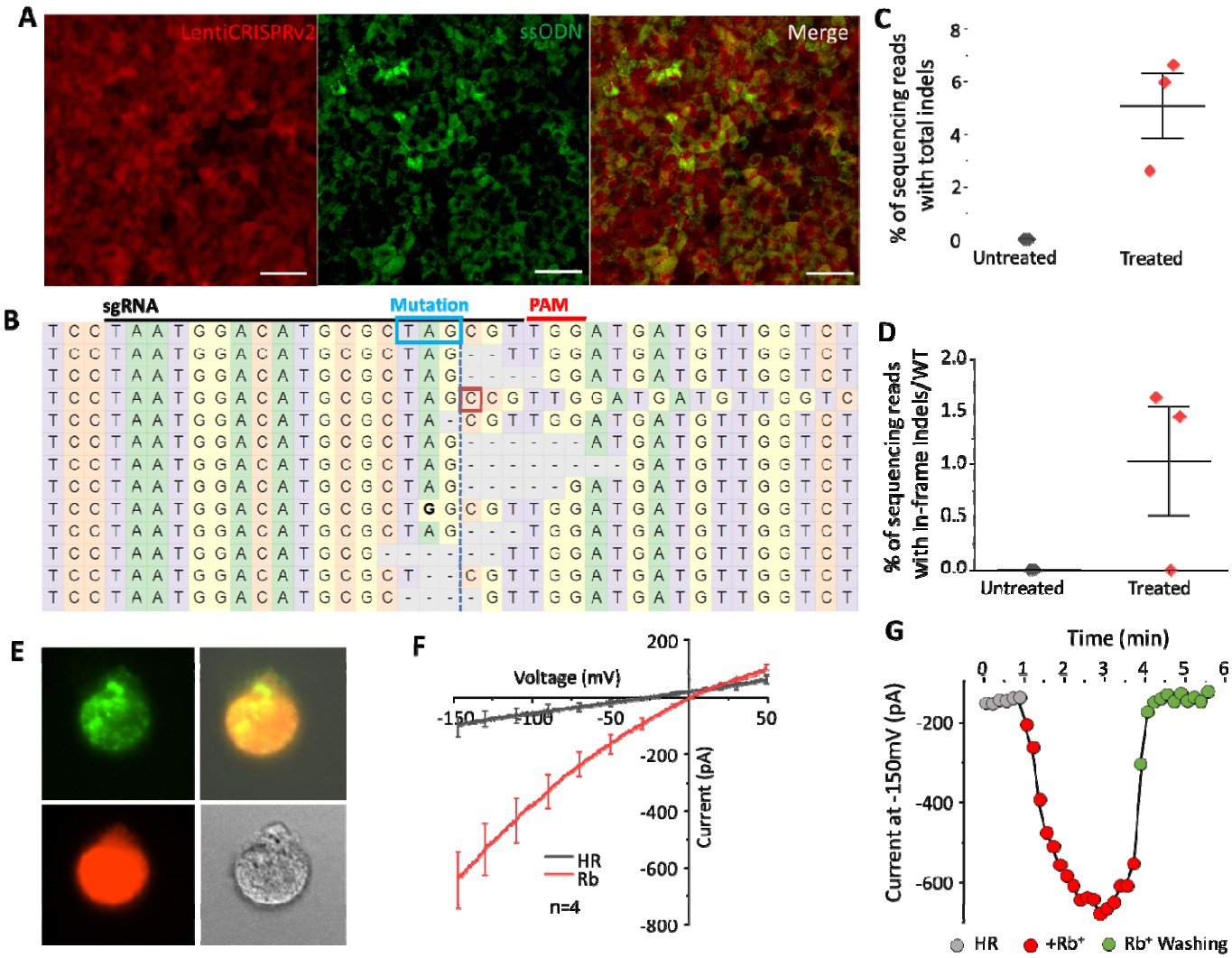

Figure 1: CRISPR-Cas9 nuclease editing outcomes in iPSC-RPE^{W53X}. *A] Transduction with LentiCRISPRv2 –mCherry carrying Cas9 and sgRNA (red panel) and delivery of ssODN-ATTO488 via SNCs (green panel) in iPSC RPE^{W53X} showing the dual fluorescence (merged panel). B] Deep sequencing reads from cells that received both LentiCRISPRv2 and ssODN treatment shows the nucleotide distribution around the DSB cleavage site (vertical dashed line). The sgRNA protospacer location is highlighted by a black line, protospacer adjacent motif (PAM) by a red line, and pathogenic early stop codon (TAG) mutation in the blue box. Substitutions are highlighted in bold, insertions are shown in red boxes, and deletions are shown by a dash. C] Total percentage of sequencing reads containing indels at the DSB site across the treated samples (n=3, biological replicates). D] Percentage of reads comprised of WT reads and in-frame indels observed in the treated samples (n=3, biological replicates). E] Fluorescence microscopy image of a single dissociated iPSC-RPE cell expressing both reporters, chosen for manual patch-clamping. F] Representative patch-clamp recording of K^+ current from the edited cell shown in Fig 1E. The grey line indicates the current recorded in the ringer solution, while the red line indicates the current measurement in presence of Kir7.1 activator, Rb^+ ion. This patch-clamp recording is representative of 4 single cells. G] Time course measurement showing the current increment at rest in Ringer's solution (HR, grey), through 140mM Rb^+(red) stimulation, and subsequent restoration of physiological K^+ current after washing (green).*

2. Validation of ABEs in HEK^{W53X}cell line confirms the activity and specificity of ABE8e mRNA

Given the relatively low efficiency and heterogeneous outcomes of the nuclease-mediated gene editing approach tested above, we next explored base editing as an alternative strategy to correct the W53X mutation. CRISPR base editors are engineered effectors that utilize the programmable DNA targeting ability of Cas9 to deliver a nucleotide base-modifying enzyme to a precise editing window, leading to the targeted conversion of one or more bases and resulting in an altered DNA sequence without introducing DSBs or relying on cellular DNA repair machinery. The W53X mutation is caused by the *KCNJ13*, c.158G>A nucleotide change, and therefore an ABE-mediated base editing strategy has potential to correct the mutation through an A>G conversion. To screen ABEs and validate the sgRNA for their ability to edit this pathogenic locus with functional restoration of Kir7.1 channel, we generated HEK^{W53X} cells that stably express *KCNJ13*^{W53X}-GFP and an isogenic wild-type control line, HEK^{WT}-GFP in which the wild-type *KCNJ13* sequence was inserted into the FRT site [Fig 2A, 2B]. We chose the ABE8e base editing effector due to its high efficiency (*35, 41*) and based on estimated editing window at protospacer positions 4-8, counting PAM as position number 21-23. We used three bioinformatic tools for sgRNA design (see Methods). Only one sgRNA (G*C*G*CUAGCGUUGGAUGAUGU, PAM; TGG) satisfied our specificity requirements while also placing the c158G>A position within the editing window of ABE8e [Fig2C]. We tested the activity of ABE8e BE in mRNA and protein forms. HEK^{W53X} cells were electroporated with either a mixture of ABE8e mRNA and sgRNA, or with ABE8e: sgRNA RNP complexes. Deep sequencing analysis was done on the treated cells by isolating RNA instead of DNA, to distinguish the inserted allele from the endogenous allele. The pool of electroporated HEK^{W53X} cells showed significantly higher AT to GC correction efficiency with ABE8e mRNA (50.29 ± 1.38%) compared to ABE8e RNP (31.44 ± 3.39%) [Fig 2D]. Our on-target analysis showed minimal indels introduced at and around the protospacer, as expected for this base editing approach [Fig 2E].

The W53X nonsense mutation in *KCNJ13* disrupts its protein expression in HEK^{W53X} cells, so we next assessed whether base editing restored Kir7.1 expression at the protein level. Immunocytochemistry demonstrated that Kir7.1 protein is present in the membrane in most of the base edited HEK^{W53X} cells,

similar to control HEK^{WT} cells. On the other hand, in untreated HEK^{W53X} cells, the signal is accumulated in the nucleus due to its premature truncation [Fig 2F]. These results confirmed the successful translation and trafficking of full-length protein after the editing [Fig 2F].

To test the Kir7.1 channel function, whole-cell currents were recorded from pools of base-edited $HEK^{W53X\text{-}BE}$ cells, untreated HEK^{W53X} mutant cells, and untreated HEK^{WT} cells using an automated patch-clamp system [Fig 3A-C]. In a standard external physiological Ringer's solution, HEK^{WT} cells had a large negative membrane potential (-74.24 ± 4.16 mV, n=3 individual cells) (Supplementary Figure 4a). They exhibited an inward rectifying average Kir7.1 current of -19.6 ± 4.15 pA (n=26 individual cells) at -150 mV in 5 mM K^+. The inward current was stimulated in response to external 140 mM Rb^+ (a known activator of Kir7.1 channel) by 7.5-fold (-146.65 ± 30.13 pA), which is characteristic of Kir7.1-mediated current [Supplementary Fig 4B]. However, the current was not blocked by adding 20 mM Cs^+ (a known blocker of Kir7.1 channel) to bath solution (-19.0 ± 3.58 pA), suggesting a low Cs^+ sensitivity of the Kir7.1 channel [Fig 3A]. These responses were not observed in untreated HEK^{W53X} mutant cells, which had a significantly lower resting current amplitude (-9.71 ± 1.26 pA) and negligible change upon addition of Rb^+ or Cs^+ [Fig 3B]. Importantly, base-edited $HEK^{W53X\text{-}BE}$ cells exhibited restored full-length Kir7.1 protein in 80% of cells (n=60) and the characteristic Rb^+-responsive K^+ current (-33.33 ± 7.68 pA baseline; -415.22 ± 54.0 pA with Rb^+, -42.19 ± 9.56 pA with Cs^+) [Fig 3C]. The K^+ current profile of 20% of the treated HEK^{W53X} cells (n=15) was comparable to HEK^{W53X} untreated cells, which we attribute to unedited cells (K^+ current in Ringer's; -30.92 ± 8.04 pA, Rb^+; -57.67 ± 12.46 pA, Cs^+; -13.89 ± 5.07 pA) [Fig 3C]. From these preliminary experiments, we conclude that ABE8e mRNA + sgRNA delivery is capable of correcting the W53X mutation at high efficiency (around 50%), restoring Kir7.1 protein levels and K+ conductance.

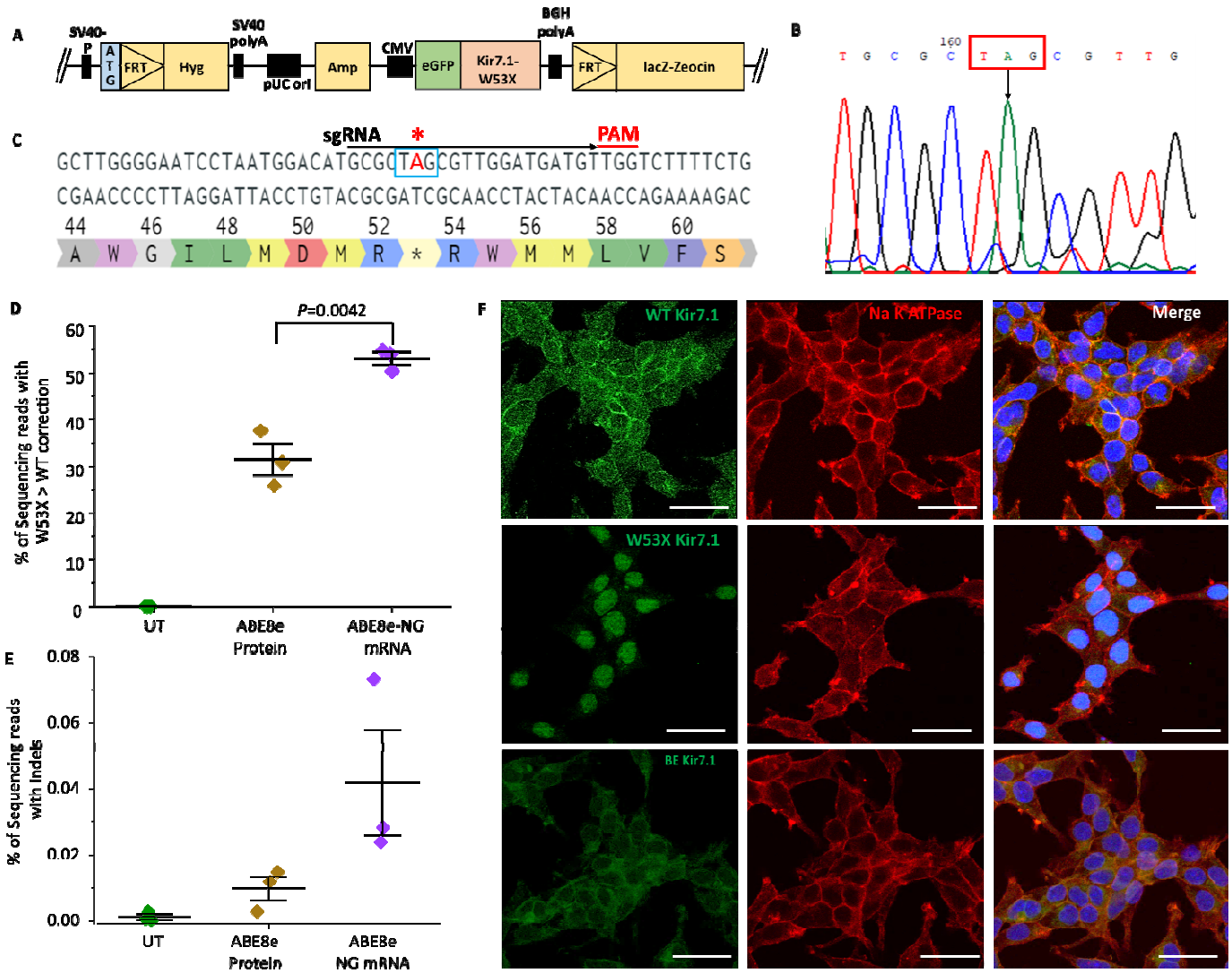

Figure 2: Evaluation of ABE8e RNP and ABE8e mRNA to correct hKCNJ13$^{W53X/W53X}$ allele in HEK293 FRT stable cells. *A] Construct design to generate HEK293 FRT stable cells harboring the KCNJ13^{W53X}* allele. *B] Schematic of the hKCNJ13 locus highlighting the mutation c.158G>A (in blue box marked with *) and position of the W53X targeting sgRNA (black line) with TGG PAM (red line). C] Chromatogram generated from HEK293 FRT stable cells showing the W53X codon marked in the red box and the downward black arrow showing the specific nucleotide change (G>A). D] Base editing efficiencies shown as percentage of sequencing reads with the corrected WT allele (and no other silent changes, bystander edits, or indels) in HEK293^{W53X} cells following electroporation of ABE8e protein + sgRNA (RNP) or ABE8e mRNA + sgRNA (n=3). Markers (diamonds) represent the individual biological replicates (n=3), and error bars represent SEM. E] % of sequencing reads with indels in ABE8e RNP and ABE8e mRNA treated stable cells (n=3). Markers (diamonds) represent the individual biological replicates (n=3), and error bars represent SEM. F] Kir7.1 expression in ABE8e mRNA treated cells assessed by immunocytochemistry. GFP primary antibody was used to enhance the endogenous signal. DAPI was used to stain nucleus. Scale bar; 50* μm.

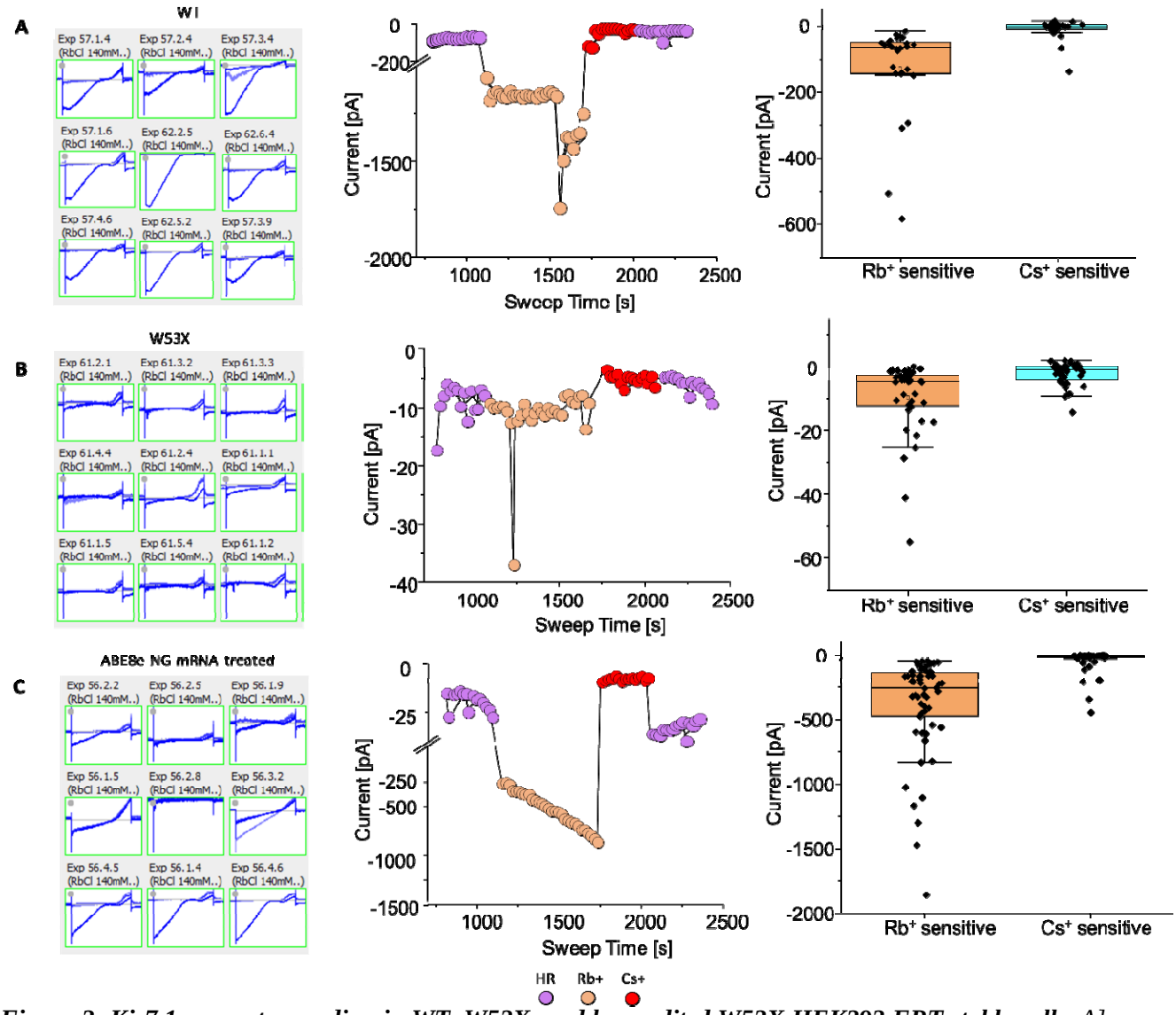

Figure 3: Kir7.1 current recording in WT, W53X, and base edited W53X HEK293 FRT stable cells. *A] Snapshot of Kir7.1 current profile in WT stable cells. Current-Sweep plot is shown for one representative cell. Rb^+ and Cs^+ sensitive current in HEK^{WT} stable cells B] Snapshot of Kir7.1 current profile in HEK^{W53X} stable cells. Current-Sweep plot is shown for one representative cell. Rb^+ and Cs+ sensitive current in HEK^{W53X} stable cells. C] Snapshot of Kir7.1 current profile in $HEK^{W53X\text{-}BE}$ cells using ABE8e mRNA. Current-Sweep plot is shown for one representative cell. Rb^+ and Cs+ sensitive current in $HEK^{W53\text{-}BE}$cells.*

3. **Efficient ex vivo base editing in patient specific fibroblasts using SNC-encapsulated ABE.**
Since LCA16 is a progressive, degenerative disease, any in vivo gene editing approach would have to be conducted in early life before the retina has significantly degenerated. On the other hand, ex vivo gene correction in patient-derived cells could be used to generate implantable autologous RPE cell therapies for patients whose retinas have already degenerated past the point of in situ therapeutic intervention. To

explore this possibility, we encapsulated ABE8e mRNA and sgRNA in SNC-PEG nanoparticles [Fig 4A] (*31*) for delivery into fibroblasts derived from an LCA16 (W53X homozygous) patient (Fibro^{W53X}). 5 days post-treatment, we assessed base editing efficiency using deep sequencing. As expected, the higher activity of ABE8e yielded more efficient 'AT' to 'GC' editing (52.31 ± 0.06%) at the target W53X site (A^{6}). Cells from both the treated and untreated populations had low levels of other substitutions in the amplicon, including bystander A>G and random T>G, T>C, G>A substitutions, with ABE8e exhibiting 6.48 ± 1.44% unwanted substitutions, and untreated Fibro^{W53X} cells showing 2.56 ± 0.02% unwanted substitutions [Fig 4B]. Rare indel outcomes were detected in the ABE8e treated samples (2.71 ± 0.40%) [Fig 4B]. Bystander A>G editing near the target nucleotide was lower compared to random substitutions observed in the ABE8e treated samples (A^{14}; 0.26 ± 0.03%, A^{17}; 0.07 ± 0.07%) [Fig 4C]. We also observed some ABE activity upstream of the protospacer at positions A^{-2}, A^{-4}, A^{-8}, and A^{-9}. ABE8e has a wider editing window than expected, and we detected A>G transitions at A^{-9} (0.08 ± 0.08%) other than at A^{-2} (0.34 ± 0.025%) [Fig 4C]. This bystander editing within and outside the protospacer resulted in silent (L48L) and missense mutations (D50G, M51V, M56V, M57V). These mutations were observed at a very low frequency (<1%) in Fibro^{W53X} [Fig 4D], and, while unlikely, further work would be required to determine whether any of these outcomes would lead to deleterious outcomes.

We also assessed the activity of another ABE mRNA (ABE7.10max) in Fibro^{W53X} to test the state-of-the-art. The ABE7.10max also had the similar editing window at protospacer position 4-7 (PAM 21-23) and, therefore placed the mutant ‘A’ nucleotide base within the activity window. Unfortunately, the treated cells showed lower ‘AT’ to ‘GC’ editing efficiency (14.93 ± 1.73%; *p*-value = 0.000027) compared to ABE8e at the target W53X site (A^{6}). Altogether, lower activity of ABE7.10max was also reflected at other bystander ‘A’s [A^{14}; 0.09 ± 0.09%, A^{-2}; 0.07 ± 0.07%, A^{-4}; 0.15 ± 0.08%], other random substitutions (4.67 ± 0.79%) and indels (1.35 ± 0.42%) in the amplicons [Supplementary Figure 8]. This particular ABE mRNA could be advantageous in cases, where only >10% on-target corrections could do wonder while avoiding all the detrimental bystander mutations.

These results confirmed that ABEs, particularly ABE8e, can efficiently revert the endogenous W53X nonsense mutation to wild-type in patient-derived fibroblasts, providing important proof-of-concept with an eye toward autologous cell transplantation therapies.

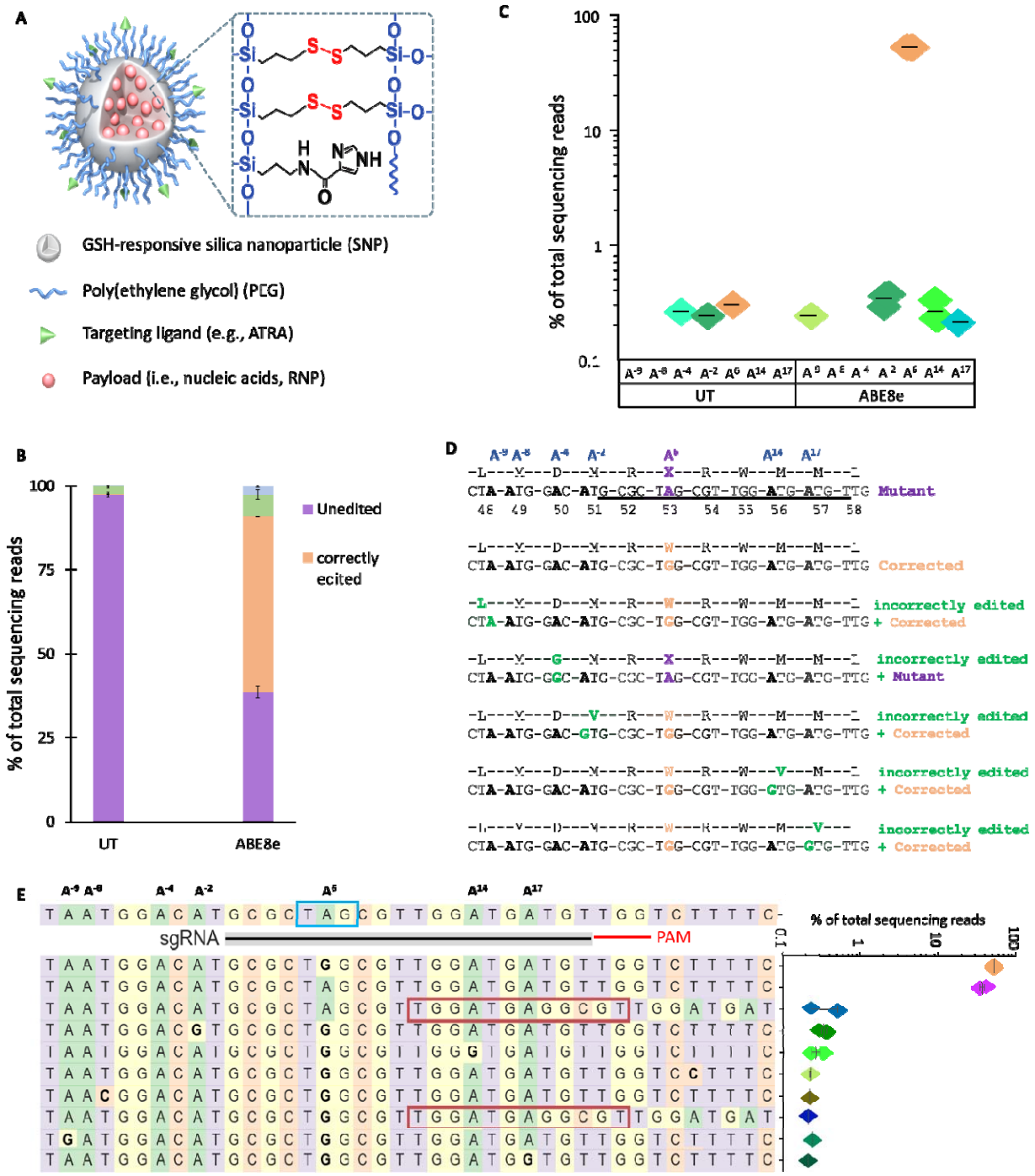

Figure 4: Evaluation of ABE mRNA + sgRNA combinations to correct the W53X allele in LCA16 patient fibroblasts. *A] Design of silica nanoparticles(34) used to encapsulate ABE8e mRNA and sgRNA. B] Base editing efficiencies shown as the % of total DNA sequencing reads, classified as unedited, correctly edited, incorrectly edited due to bystander 'A' edits, and with indels in treated and untreated (UT) cells. C] % Editing of the target (A^{6}) and bystander (A^{-9}, - A^{-8}, A^{-4}, A^{-2}, A^{14}, A^{17}) 'A' to 'G' by ABE8e mRNA as observed in three independent experiments. D] Amino acid conversion at the respective location generated due to target and bystander edits. The protospacer sequence is underlined, the pathogenic early stop codon is in a purple box, the target 'A>G' edit is marked in orange, and bystander 'A' edits are marked in green. E] The sgRNA location is marked by black line, PAM by red line, and mutation in the blue box. All the 'A' bases within the protospacer are numbered from 1-20 based on their location. The 'A' bases downstream of the protospacer are numbered from -1 to -9, considering +1 as the first base of the protospacer. The top 10 most frequent alleles generated by ABE8e mRNA treatment show the nucleotide distribution around the cleavage site for sgRNA. Substitutions are highlighted in bold, insertions are shown in the red box, and deletions are shown by dashes. The scatter plot shows the frequency of reads observed in treated cells (n=3 biological replicates). Figures presenting data from replicates are shown as mean ± SEM.*

4. Restoration of Kir7.1 channel function in edited patient-derived iPSC-RPEs.

Next, as a model for in vivo gene editing therapies for LCA16, we applied our base editing strategy to patient iPSC-derived RPE harboring the W53X mutation. Based on previous reports indicating that lipofection and AAV-mediated delivery are challenging in RPE, we used SNC-PEG as a delivery vector. We did not observe any toxicity in the ABE8e treated RPE, and its morphology was comparable to untreated iPSC-RPE^{W53X} [Fig 5A]. Deep sequencing analysis in the base edited iPSC-RPE^{W53X} revealed 17.82 ± 1.53% editing of the mutant nucleotide to the wild-type sequence following ABE8e treatment [Fig 5B]. Less than 4% of resultant alleles carried undesired mutations: indels quantified in treated RPE had a frequency of 0.68 ± 0.11% compared to 0.01 ± 0.002% in untreated controls, and bystander substitutions quantified in treated RPE totaled 2.94 ± 0.42% compared to 1.78 ± 0.07% in untreated controls [Fig 5C, Supplementary Figure 6].

A manual patch-clamp was carried out on the pool of base edited iPSC RPE^{W53X} cells [Fig 5D] to assess the functional rescue of the Kir7.1 channel. Importantly, in contrast to the patch-clamp assays above that were performed on sorted cells that received editing machinery, these assays were performed on the entire cellular pool dissociated into single cells since there was no reporter or selection marker to aid in identification of recipient or edited cells. Three different kinds of Kir7.1 current profiles were observed in the edited iPSC-RPE^{W53X} pool. Some of the cells (n=5) showed a normal amplitude of K^{+} conductance (-101.98 ± 0.07 pA) in Ringer's solution, which was potentiated in Rb^{+} external solution by 8-fold (-

820.97 ± 265.54 pA). These were the high responding cells in the pool that showed rescue of Kir7.1 channel function and were most likely to have only W53X>WT correction. Some of the cells did not show any recovery of Kir7.1 current (Ringer's; -33.66 ± 31.59 pA, Rb^+; -80.51 ± 19.37 pA) and had a similar profile as iPSC RPE^{W53X} cells (*11*). These low responding cells (n=4) likely experienced no base editing. A few cells showed slightly higher Rb^+-stimulated current than the untreated iPSC-RPE^{W53X} cells, but not like iPSC-RPE^{WT} cells. These were the medium responding cells that showed only a 3-fold Rb^+ response (-238.74 ± 102.13 pA) for the current amplitude observed in Ringer's solution (-72.57 ± 29.74 pA). We hypothesize that medium responding cells contain a bystander edit in addition to the targeted gene correction, or alternatively that correctly base edited *KCNJ13* is lowly expressed in these cells. The current-sweep plots of the representative cell under different treatment solutions are shown in Fig 5E.

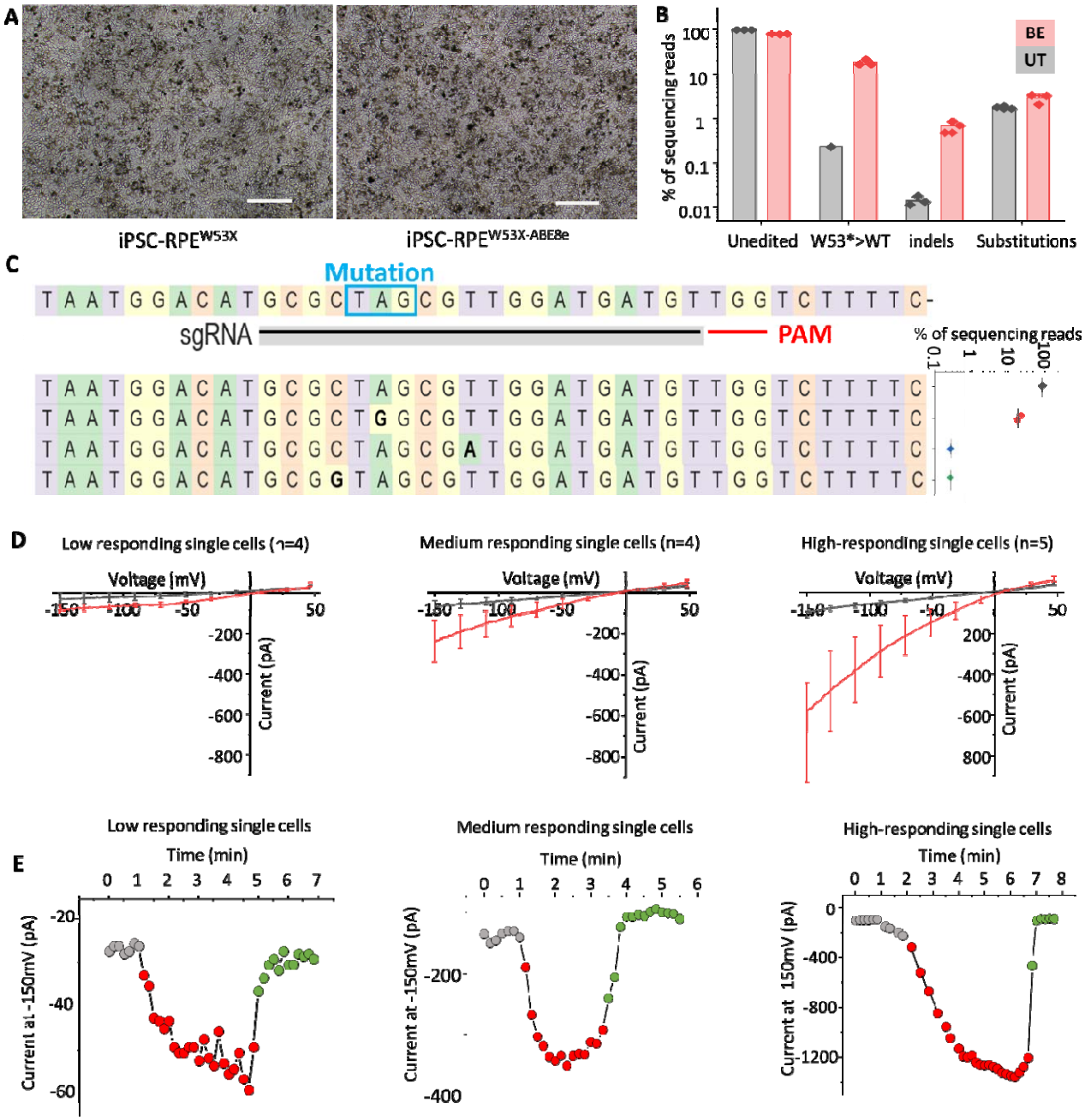

Figure 5: Evaluation of ABE8e to correct W53X allele in iPSC-RPE^{W53X}. *A] Representative bright-field images of base editor treated and untreated iPSC RPE^{W53X}. B] Base editing efficiencies following treatment (BE) with ABE8e mRNA and sgRNA encapsulated in SNC-PEG in iPSC- RPE^{W53X} as compared to untreated (UT) cells C] Reads generated by ABE8e mRNA treatment showing the nucleotide distribution around the cleavage site for sgRNA. Substitutions are highlighted in bold. The scatter plot shows the frequency of alleles observed in treated cells (n=3). Lines and error bars are represented as mean ± SEM. D] Manual single-cell patch-clamp assays on iPSC-RPE^{W53X} cells after treatment with ABE8e. Of the 13 cells measured, each could be binned into one of 3 classes: low responding single cells, which appeared to be unedited mutant cells, medium responding single cells, which showed a low level of Rb^+ response, and high responding single cells, which showed Rb^+ response like iPSC-RPE^{WT} cells. The*

number (n) of cells binned into each class is shown at the top of each graph. E] Current-sweep plot from a representative cell of each bin across a time course of being exposed to physiological Ringer's solution (gray), Rb^+ stimulation (red), and subsequent wash with Ringer's solution (green).

5. In vivo base editing partially rescues Kir7.1 functions and ERG phenotype in LCA16$^{W53X/-}$ mice.

A significant limitation to translating our *KCNJ1*^{W53X} gene correction strategy to preclinical models is the lack of a mouse model harboring a homozygous pathogenic mutation in the gene. Unlike in humans, *Kcnj13* is an essential gene in the mouse – at least one normal allele is required for survival beyond postnatal day 1 (*7, 42*), precluding the establishment of a genetic model recapitulating the human recessive disease. To overcome this limitation, we started with a heterozygous *Kcnj13*$^{W53X/+}$ mouse (REF) and disrupted the remaining WT *Kcnj13* allele only in RPE after birth using CRISPR-Cas9 RNPs encapsulated in SNC-PEG-ATRA via subretinal injections. Before the disruption, a full field scotopic ERG was performed on *Kcnj13*$^{W53X/+}$ mice to assess the normal visual function. The amplitude of the a-wave, b-wave, and c-wave of the scotopic ERG for these mice were 157.76 ± 20 µV, 380.9 ± 57.3 µV at 10 cd.s/m^{2,} and 350.93 ± 31.16 µV at 25 cd.s/m^2 respectively. After treatment with Cas9 nuclease targeted to disrupt the WT allele, mice acquired an LCA16 phenotype, characterized by significant reduction in c-wave amplitude. Two weeks following injection of RNPs, a decrease in a-wave, b-wave, and c-wave amplitudes was observed. The a-wave and b-wave recovered somewhat after 4 and 6 weeks, but the c-wave, which correlates with RPE cell function, had an almost 70 % reduction in amplitude in all follow-up ERGs (*40*). These mice, with the reduced or absent ERG c-wave, were then used as an LCA16 model (*Kcnj13*$^{W53X/-}$) to validate our in vitro findings.

We designed sgRNAs targeting the WT or W53X alleles of mouse *Kncj13* and packaged them together with ABE8e mRNA and GFP mRNA into SNC-PEG-ATRA. After subretinal injection into *Kcnj13*$^{W53X/-}$ mice, the injection site could be located through GFP fluorescence [Fig 6C], and GFP-positive RPE tissue was dissected for deep sequencing of the *Kcnj13* locus. We found that 3 µg ABE mRNA was approximately twice as efficient as 2 ug, resulting in just under 10% editing (9.48 ± 3.26% for 3 ug compared to 4.73 ± 2.51% for 2 ug, n=4 eyes for each dose) [Fig 6D]. Our on-target analysis showed no other A>G substitutions outside or within the protospacer region, but indels mutations (2 µg: 0.04 ±

0.002%, 3 μg: 0.04 ± 0.0007%) were observed at a very low frequency, similar to placebo (PBS/ empty SNC-PEG-ATRA; 0.03 ± 0.01%) treated mice [Fig 6E].

The *Kcnj13*$^{W53X/-}$ base edited mice were subjected to ERG to assess the functional outcomes of editing. These mice (n=3 eyes) underwent ERG monitoring at 2, 4, 8, 12, and 20 weeks following base editor treatment. In the 2nd week following the injection, the amplitude of a-, b-, and c- waves measured 23.45 ± 3.44, 50.29 ± 12.82, and 37.22 ± 14.75 μV respectively. The amplitudes of the a-wave and b-wave were 41.51 ± 9.9 μV and 82.5 ± 21.8 μV at the week 4 ERG, respectively, and remained consistent in the follow-up ERGs at weeks 8, 12, and 20. The c-wave amplitude at week 4 measured 68 ± 42.76 μV, which increased to 137.57 ± 60.14 μV at week 8, 139.85 ± 22 μV at week 12, and 153.22 ± 75.12 μV at week 20. These data demonstrate the phenotypic reversal of mutant RPE following base editing by ABE8e encapsulated SNC-PEG-ATRA.

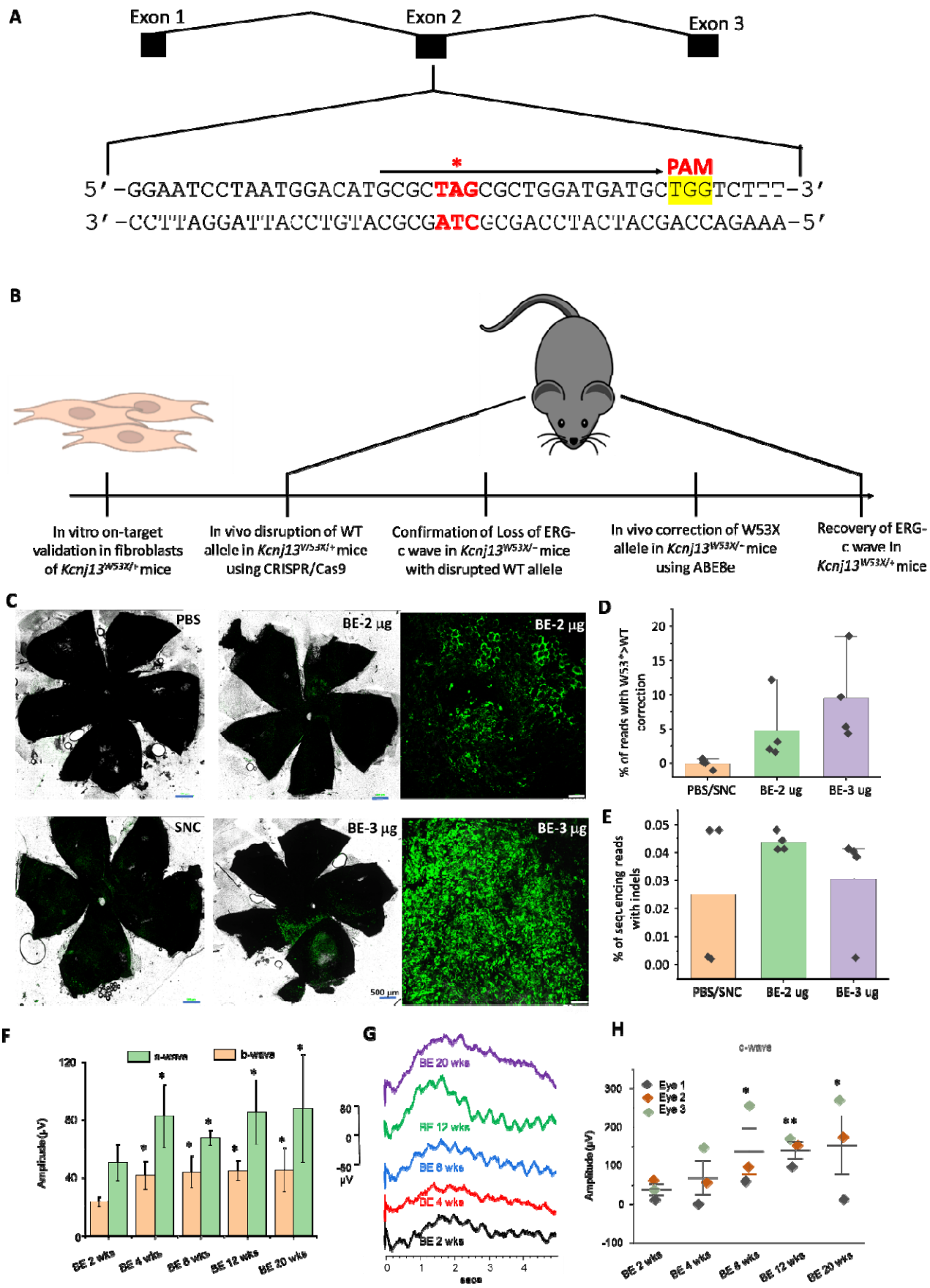
A
Exon 1
Exon 2
Exon 3
*
PAM
5′-GGAATCCTAATGGACATGCGCTAGCGCTGGATGATGCTGGTCTTT-3′
3′-CCTTAGGATTACCTGTACGCGATCGCGACCTACTACGACCAGAAA-5′
B
In vitro on-target validation in fibroblasts of Kcnj13W53X/+ mice
In vivo disruption of WT allele in Kcnj13W53X/+ mice using CRISPR/Cas9
Confirmation of Loss of ERG-c wave in Kcnj13W53X/- mice with disrupted WT allele
In vivo correction of W53X allele in Kcnj13W53X/- mice using ABE8e
Recovery of ERG-c wave in Kcnj13W53X/+ mice
C
PBS
BE-2 µg
BE-2 µg
SNC
BE-3 µg
BE-3 µg
500 µm
D
% of reads with W53*>WT correction
PBS/SNC
BE-2 ug
BE-3 ug
E
% of sequencing reads with indels
PBS/SNC
BE-2 ug
BE-3 ug
F
a-wave
b-wave
Amplitude (µV)
BE 2 wks
BE 4 wks
BE 8 wks
BE 12 wks
BE 20 wks
G
BE 20 wks
BE 12 wks
BE 8 wks
BE 4 wks
BE 2 wks
µV
secs
H
c-wave
Eye 1
Eye 2
Eye 3
Amplitude (µV)
BE 2 wks
BE 4 wks
BE 8 wks
BE 12 wks
BE 20 wks

Figure 6: Phenotypic reversal of mouse RPE^{W53X} following in vivo ABE8e treatment. *A] The sgRNA design targeting the Kcnj13^{W53X} allele for base editing, with the black arrow representing the sgRNA spacer sequence, the desired base editing site indicated by an asterisk, and the PAM shown in yellow. B] Workflow of in vivo base editing strategy. C] RPE floret of eyes subretinally injected with SNC-PEG-ATRA packaged ABE8e mRNA, W53X-sgRNA, and GFP mRNA or empty SNC-PEG-ATRA/PBS as a mock treatment. D] % of sequencing reads showing the W53X>WT corrections, observed in Kcnj13$^{W53X/-}$ mice treated with 2 μg or 3 μg of ABE8e. E] % of sequencing reads showing the indels, observed in Kcnj13$^{W53X/-}$ mice treated with 2 μg or 3 μg of ABE8e. F] a-wave and b-wave amplitude measured by scotopic ERG at 10 cd.s/m2 flash stimuli on ABE8e treated Kcnj13$^{W53X/-}$ mice (n=3 eyes) at 2,4,8,12 and 20 weeks. G] Representative c-wave traces recorded at 25 cd.s/m2 from the ABE8e-injected eye demonstrated the recovery of c-wave amplitude and RPE cell function. H] Graph displaying the progressive recovery of the c-wave over time from each eye following the correction of the mutant allele with ABE8e. *Indicates p-value < 0.5* and ** indicates p-value <0.05. *Figures presenting pooled data are represented as mean ± SEM.*

6. Off-target analysis of sgRNA for human and murine W53X target confirms the target specificity

It is possible for the Cas9 moiety that dictates the specificity of a base editor to its target site to bind off-target sites in the genome based on a similarity to the guide sequence. We used an online computational algorithm, Cas-OFFinder (*38*), to identify the putative off-target sites for the sgRNA used above in our ABE treatments. The likelihood of off-target editing should be greatest at sites with 1-2 mismatches and no DNA/RNA bulge, but our in-silico analysis showed no such off-target sites for this sgRNA. We found 2727 potential off-target sites, most harboring 4 mismatches with 1 nucleotide RNA bulge (n=2004) or DNA bulge (n=512), with other configurations and closer matches occurring much less frequently (Supplementary Figure 2).

We analyzed the off-target activity of ABE8e in HEK^{W53X}, LCA^{W53X}, and iPSC-RPE^{W53X} cells at the top nine predicted sites (Supplementary Table 4). Deep sequencing analysis of these sites showed that ABE8e treatment did not lead to significant off-target A>G editing or introduction of indels compared to untreated control cells except at one locus. In particular, this one off-target (GRCh38:50530925 Intergenic) showed 4x more substitutions in only base edited HEK^{W53X} cells, which is an already reported A>G single nucleotide polymorphism (rs139941105, Minor Allele Frequency in 1000 Genomes=0.01) of no known clinical significance [Fig 7A,7B]. These data demonstrate that the off-target modification levels of ABE8e at each of nine potential sites are much lower than its on-target editing efficiency, and overall indicate a favorable off-target profile.

To detect in vivo off-target editing, we used isolated optic cup gDNA from base editor-treated heterozygous *Kcnj13*$^{W53X/+}$ mice and screened 11 top predicted off-target sites by rhAMP (Supplementary Table 6). ABE8e treatment in these mice successfully introduced on-target W53X>WT correction (9.5%). Similar to our in vitro off-target analyses described above, we detected no substantial off-target editing following in vivo editing of mouse RPE [Fig 7C, 7D]. Together, these results suggest that ABE8e could be an effective and specific method to correct polymorphisms in the genome and that SNCs can serve as effective vehicles to correct mutations in the RPE.

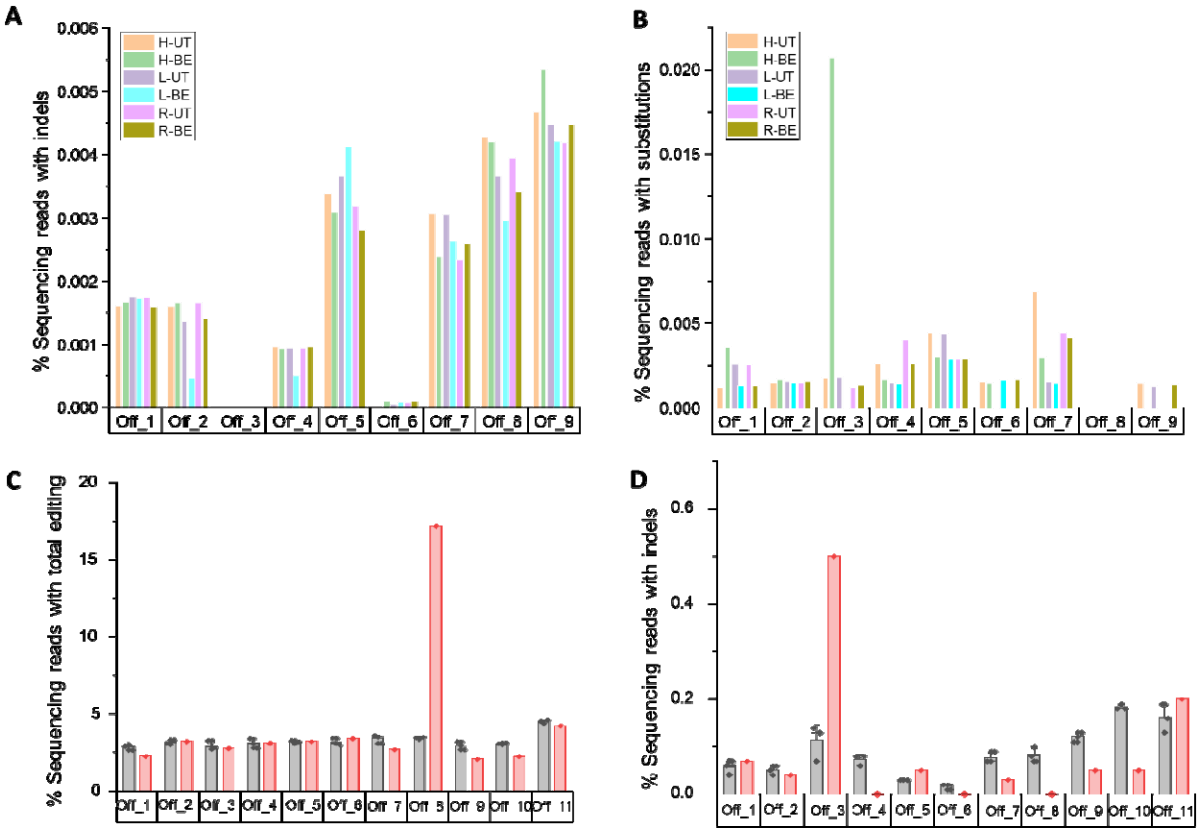

Figure 7: Off-target editing analysis in treated cells and the treated mouse eye. *A] Percentage of sequencing reads with indels as observed by deep sequencing analysis in HEK*^{W53X}*, Fibro*^{W53X,} *and iPSC RPE*^{W53X} *and their respective untreated cells (H stands for HEK293 stable cells, L stands for LCA16 fibroblasts and R stands for iPSC RPE). B] Percentage of sequencing reads with substitutions as observed by deep sequencing analysis in HEK*^{W53X}*, Fibro*^{W53X,} *and iPSC RPE*^{W53X} *and their respective untreated cells. C] Percentage of sequencing reads with total editing including substitutions and NHEJ as observed by deep sequencing analysis of optic cup gDNA from ABE8e treated Kcnj13*$^{W53X/+}$ *mice (n=3 eyes) compared to a negative control Kcnj13*$^{W53X/+}$*mouse treated only with PBS (n=1 eye). D] Percentage of sequencing reads with only indels as observed by deep sequencing analysis in ABE8e treated Kcnj13*$^{W53X/+}$ *(n=3 eyes) compared to a negative control Kcnj13*$^{W53X/+}$*mouse treated only with PBS.*

Discussion

At present, recessive loss-of-function *KCNJ13* point mutations are the only known genetic cause of LCA16, which disrupt the Kir7.1 channel function and alter the RPE physiology, leading to retinal degeneration with progressive vision loss in patients. Correcting these mutations in RPE cells could permanently restore the Kir7.1 channel function and revert the disease phenotype or prevent further disease progression. Of the 12 different known LCA16-causing mutations (*43*), 8 are theoretically accessible by base editors, and 5 of those by ABE (requiring A>G (or T>C) edits). Here, we provide important proof-of-concept that delivery of ABE to RPE via subretinal injection of SNCs can result in correction of the pathogenic allele and restoration of Kir7.1 channel function.

As an alternative strategy for patients whose RPE has degenerated past the point of meaningful correction in vivo, we also suggest that base editing of patient-derived fibroblasts can potentially provide a platform for edited iPSC-RPE derivation for autologous cell therapy.

The SNC formulation is a powerful tool for protein and nucleic acid delivery. In this study, we used SNC-PEG to deliver base editor mRNA or RNP to patient-derived fibroblasts, resulting in >50% editing efficiency, and to deliver base editor mRNA to iPSC-RPE, achieving 18% editing. For in vivo editing of mouse RPE, we used the ligand-conjugated SNC-PEG-ATRA and observed 10% editing efficiency. In all cases, base edited cells or tissues exhibited significant functional rescue of the Kir7.1 channel. Like many other ocular diseases, treating LCA16 should not require the correction of all the mutant cells. We previously showed that the pathological state of RPE can be reversed by rescuing 25% of the Kir7.1channel function (*11*). A recent trial from Editas (Edit101) introduced indels in the *CEP290* gene that causes a different type of Leber Congenital Amaurosis, LCA10, and restored visual function in non-human primates with >10% functional photoreceptors (*44*). The base editing efficiencies we achieved in this study are therefore well within the range of providing considerable therapeutic benefit.

Our study answers important questions about the efficacy of allele targeting and the delivery of editing tools to murine RPE. The most significant outcome of this research is the proof that in vivo editing can restore RPE function. The edited mice exhibited partial recovery of the ERG c-wave amplitudes with no

further retinal degeneration, indicating the need of further studies to determine the extent to which this treatment prevents further vision loss or improves visual function. .

One limitation of our study is that we do not yet know the clonal editing outcomes of cells edited in vitro or in vivo. The combination of alleles in a single cell is a critical parameter for the function of the tetrameric Kir7.1 channel. Correction of just a single allele while having detrimental edits in some of the second allele will likely not restore RPE health to as high a level as a biallelic correction. A clonal analysis would reveal the precise editing outcomes per cell and could distinguish the phenotypic impact of these edited genotypes (*45*).

In conclusion, our study addressed several major challenges in correcting an LCA16-causing pathogenic mutation in the Kir7.1 channel. Importantly, base editing of $KCNJ13^{W53X}$ in vitro and in vivo showed specificity for W53X mutation without generating detrimental on-target bystander substitutions and indels or off-target edits elsewhere in the genome, unlike a CRISPR-Cas9 HDR strategy. K^+ conductance in iPSC-RPE in vitro and ERG responses in murine RPE in vivo confirmed the functional rescue of the Kir7.1 channel following base editing. The specific delivery of base editor tools to RPE via the non-viral SNC platform provides a powerful emerging tool for tissue-specific delivery of mRNA or protein-based gene editing therapeutics with good biocompatibility, ability to package large cargo, and significantly streamlined manufacturing. Altogether, these advances pave the way for future preclinical and clinical applications of base editing for correcting mutations causing LCA16 and other ocular genetic diseases.

Acknowledgments

We thank the Stem Cell & Regenerative Medicine Center (SCRMC) fellowship for the funding support to Meha Kabra. We acknowledge Retina Research Foundations Kathryn and Latimer Murfee Chair (KS), and M.D. Matthews Research Professorship (BRP). Research was also supported by UW-Partnership Education and Research Committee funds and Harrington Discovery Institute's Gund-Harrington Scholar (KS). We thank the Helen Hay Whitney Foundation, HHMI, and the K99 award HL163805 for support to GAN. This work was supported by NIH awards NIH R01 EY024995 and R24 EY032434 (BRP), U01 AI142756, RM1 HG009490, and R35 GM118062 (DRL).

Competing interests

The authors have filed patent applications for gene editing technologies. D.R.L. is a consultant for Beam Therapeutics, Pairwise Plants, Prime Medicine, Chroma Medicine, and Nvelop Therapeutics, companies that use or deliver genome editing or genome engineering technologies, and owns equity in these companies.

Supplementary tables

Supplementary Table 1: Primers for in-fusion cloning of *KCNJ13* in FLP-In™ expression vector

Primer name	Sequence (5'-3')	GC %
In-fusion FP	TCACTATAGGGAGACCCAAGCTGGCTAGCGTTTAAACTTAatggtgagcaagggcgagga	50.0
In-fusion RP	AGTCGAGGCTGATCAGCGGGTTTAAACGGGCCCTCTAGACttattctgtcagtcctgttt	50.0
GFP FP	CAAGTCCGGACTCAGATCTCGAGCTC	57.1
Kir7.1 RP	TTATTCTGTCAGTCCTGTTT	72.7

FP: Forward primer, RP: Reverse primer. Primers for in-fusion cloning were designed using the Gibson assembly primer design tool available at https://tools.sgidna.com/gibson-assembly-primers.html and ordered from IDT (https://www.idtdna.com). The homology sequence is in uppercase, and the annealing sequence is in lowercase. The primers for Sanger sequencing (GFP FP and Kir7.1 RP) were designed using the NCBI Primer-BLAST tool (https://www.ncbi.nlm.nih.gov/tools/primer-blast/).

Supplementary Table 2: Primers to genotype mice

Primer name	Sequence (5'-3')	GC %
mKcnj13-FP	TAAATCAGCTACGGGCTAACA	42.86
mKcnj13-RP	CTGTGATAAAAGCCTCTAGCA	42.86

The primers were designed using the NCBI Primer-BLAST tool (https://www.ncbi.nlm.nih.gov/tools/primer-blast/). Annealing temperature 55 °C.

Supplementary Table 3: Primers to amplify the *hKCNJ13* on-target sites

Primer name	Sequence (5'-3')	GC %
NGS-hKCNJ13-FP	TCAAATGGATGGCGCTCAAAGA	45.0
NGS-hKCNJ13-RP	ATACCAGAGCACTGCAAAGACAA	43.0

The primers were designed using the NCBI Primer-BLAST tool and ordered along with an adaptor sequence for Illumina NGS platform from IDT. Adaptor sequence for FP: 5'-ACACTCTTTCCCTACACGACGCTCTTCCGATCT-3'Adaptor sequence for RP: 5'-GTGACTGGAGTTCAGACGTGTGCTCTTCCGATCT-3'.

Supplementary Table 4: Putative off-targets sites of human-sgRNA identified using Cas-OFFinder

S. No.	Location	Chr	strand	mismatches	G	C	G	C	T	A	G	C	G	T	T	G	G	A	T	G	A	T	G	T	T	G	G
1	STK24	13	-	3	·	T	·	·	·	·	·	·	C	·	·	·	·	·	·	·	T	·	·	·	G	G	G
2	GRCh38:133058732 Intergenic	10	-	3	·	·	A	·	G	·	·	G	·	·	·	·	·	·	·	·	·	·	·	·	T	A	G
3	GRCh38:50530925 Intergenic	18	-	2	·	G	·	·	·	·	C	·	·	·	·	·	·	·	·	·	·	·	·	·	C	A	G
4	PPM1K Intronic	4	+	3	·	·	·	A	G	·	·	·	T	·	·	·	·	·	·	·	·	·	·	·	T	G	G
5	AP2B1 Intronic	17	-	4	·	·	·	·	·	T	·	·	T	·	·	·	T	·	·	·	·	·	·	·	G	G	G
6	TMEM117 Intronic	12	+	4	·	·	.	.	·	T	T	·	T	·	·	T	·	·	·	·	·	·	·	·	T	G	G
7	GRCh38:113728054 Intronic	4	+	4	·	·	·	G	·	·	·	A	·	·	G	·	·	·	G	·	·	·	·	·	G	G	G
8	HRH1 Intronic	3	-	4	·	·	·	·	·	G	·	A	·	·	·	·	T	·	·	·	C	·	·	·	G	G	G
9	GRCh38:55352815 Intergenic	12	-	3	·	·	·	·	·	·	·	·	T	A	·	·	·	T	·	·	·	·	·	·	T	G	G

Supplementary Table 5: Primers to amplify the off-target sites of human-sgRNA

S. No.	**Primer name**	**Sequence (5'-3')**	**GC %**
1	STK24_NGS_F	GGGATGCCACTTGGAGAACT	55.0
	STK24_NGS_R	ATTCTGGGTACACACTCCCA	50.0
2	ING_CHR10_NGS_F	CAGAGAGCTCCTTCTTTCTCTGA	47.83
	ING_CHR10_NGS_R	AAGCTCCTTCCCCAAGCAAA	50.0
3	ING_CHR18_NGS_F	TGTAATGGTGATCTAGTCACAGAG	41.67
	ING_CHR18_NGS_R	GCCTCATTCTGAAAGGGTCC	55.0
4	PPM1K_NGS_F	CCACTGCAGGTAGAGCTGTT	55.0
	PPM1K_NGS_R	CTGCACTCAAGCTGGGTTTC	55.0
5	AP2B1_NGS_F	TGAGCTCTTCCTGTAAGTGACC	50.0
	AP2B1_NGS_R	TGCATACCTTTGATGGCCTG	50.0
6	TMEM117_NGS_F	GTAGGTTCAATTTCTAACCCTTGC	55.0
	TMEM117_NGS_R	AGAGGAGAAATAGGAAGCAAAGT	55.0
7	INTRONIC_CHR4_NGS_F	TGAAGTCCAAGAAAAGGCAAA	38.0
	INTRONIC_CHR4_NGS_R	CCTCCCCAAACTGAATACAAAA	41.0
8	HRH1_NGS_F	GGGTACATGGCTATTGAGTAGG	50.0
	HRH1_NGS_R	GCCACCAGTTATGGCTCACT	55.0
9	ING_CHR12_NGS_F	CATGATAACTGTGGTGCGCT	50.0
	ING_CHR12_NGS_R	GTGACCTAAATCAGTTGGATGGAG	45.83

The primers were designed using the NCBI Primer-BLAST tool and ordered along with an adaptor sequence for Illumina NGS platform from IDT. Adaptor sequence for FP: 5'-ACACTCTTTCCCTACACGACGCTCTTCCGATCT-3'Adaptor sequence for RP: 5’-GTGACTGGAGTTCAGACGTGTGCTCTTCCGATCT-3'.

Supplementary Table 6: Potential off-target sites of mouse W53X-sgRNA identified using Cas-OFFinder

S. No	#Bulge type	crRNA	DNA	Chr	Position	Strand	Mismatches	Bulge Size
1	DNA	GCGCTAGCGCTGGAT-GATGCNRG	GCaCTAGgGCTGGATGGATGCAAG	chr5	27794505	-	2	1
2	X	GCGCTAGCGCTGGATGATGCNRG	GgtCcAGCGCaGGATGATGCTGG	chr2	30011064	+	4	0
3	RNA	GCGCTAGCGCTGGATGATGCNRG	GgGCgAGC-CTGGATGATGCTGG	chr2	74762664	-	2	1
4	RNA	GCGCTAGCGCTGGATGATGCNRG	GttCTAGC-CTGGATGATGCAAG	chr2	116880781	-	2	1
5	X	GCGCTAGCGCTGGATGATGCNRG	GCtCaAGCtCTGGtTGATGCCAG	chr17	47011867	+	4	0
6	X	GCGCTAGCGCTGGATGATGCNRG	GgGCTAGCGCTGGATGcTGCTGG	chr16	38496875	-	2	0
7	X	GCGCTAGCGCTGGATGATGCNRG	GCcCTcGgGaTGGATGATGCAAG	chr9	103261947	+	4	0
8	X	GCGCTAGCGCTGGATGATGCNRG	GtGCTAtCtCTaGATGATGCCAG	chr6	134150494	+	4	0
9	X	GCGCTAGCGCTGGATGATGCNRG	GCGCTAGCcCTGGATGgTGgTGG	chr11	97642214	-	3	0

10	X	GCGCTAGCGCTGGATGATGCNRG	GCtaTgGtGCTGGATGATGCTGG	chr3	28240364	+	4	0
11	DNA	GCGCTAGCGCT-GGATGATGCNRG	GCGCTAGCGCTGGGAgGgTGCTGG	chr7	93020838	-	2	1

Supplementary Table 7: sgRNA design using CRISPR-RGEN and PnB Designer

CRISPR Target (5'-3')	PAM	AA sequence	Direction	GC contents (% w/o PAM)
AACGC**T**AGCGCATGTCCATT	AGG	**C**AG **Q**	-	50.0
TAATGG**A**CATGCGCTAGCGT	TGG	ATGG**G**C M **G**	+	50.0
GCGCT**A**GCGTTGGATGATGT	TGG	T**G**G **W**	+	50.0

The sgRNAs were designed using CRISPR-RGEN tool available at http://www.rgenome.net. The letters highlighted in red are the targeted nucleotide base using the protospacer. Amino acids listed in blue would create a missense mutation, while in green would create the desired amino acid change to make a WT Kir7.1 protein.

Protospacer	PAM	EditPos.	Base.Editor
GCGCT**A**GCGTTGGATGATGT	TGG	6	ABEmax/ABE8e
ATGCGCT**A**GCGTTGGATGAT	GTTGGT	8	SaKKH-ABEmax/ABE8e

The sgRNAs were designed using PnB Designer available at https://fgcz-shiny.uzh.ch/PnBDesigner/. Letters highlighted in red are the targeted nucleotide base using the protospacer and BE.

Supplementary Table 8: sgRNA design for mouse *Kcnj13* using Benchling.

Strand	sgRNA	PAM	Purpose	On-target score	Off-Target score
+	GAATCCTAATGGACATGCGC	TGG	WT disruption	56.6	48.4
+	GCGCTAGCGCTGGATGATGC	TGG	W53X editing	57.1	82.9

Supplementary Figures

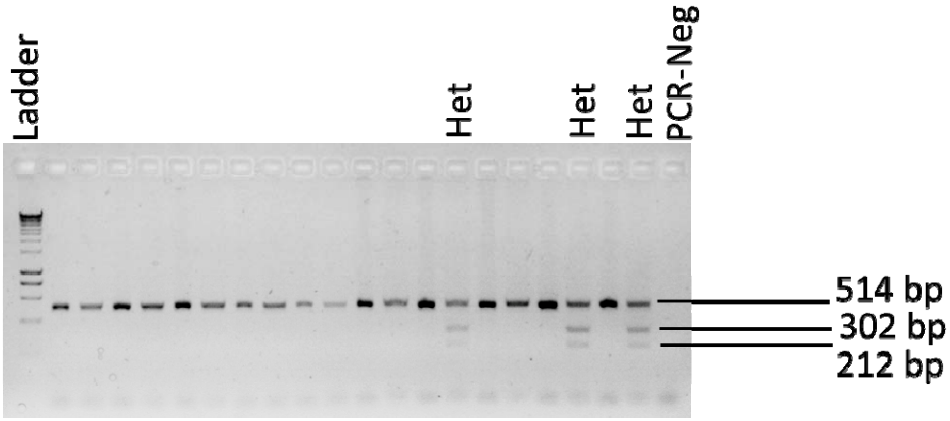

Supplementary Figure 1: Agarose gel electrophoresis showing the differences in W53X heterozygous and WT mice. *W53X mutation creates a restriction site for NheI; therefore, the W53X allele resulted in two (212 bp and 302 bp) fragments while the WT allele only one (514 bp) fragment.*

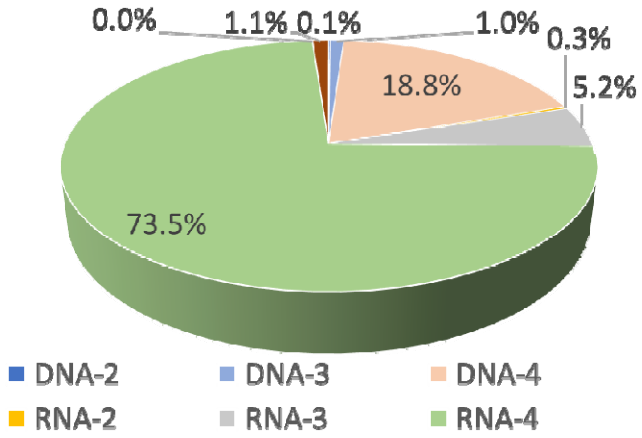

Supplementary Figure 2: Genomic off-target sites for human W53X sgRNA*. The sites were identified using standard criteria, up to 1-4 mismatches and DNA/ RNA bulge (size=1 nucleotide).*

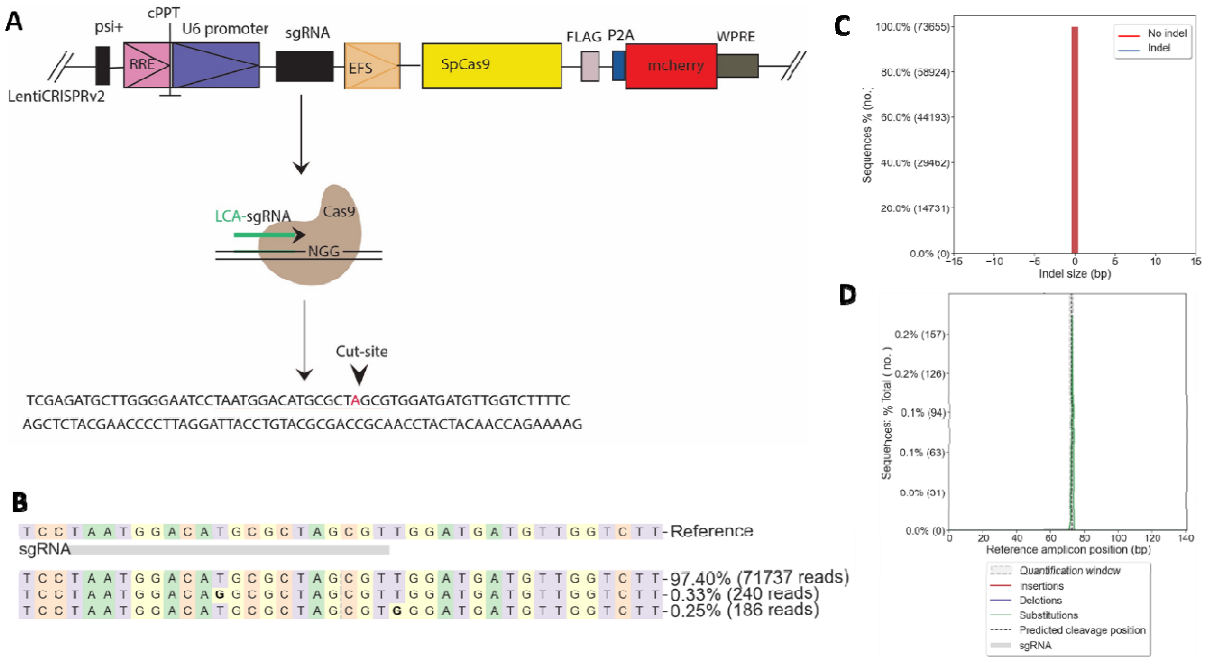

Supplementary Figure 3: Gene editing strategy and sequencing readouts from untreated iPSC RPE^{W53X}. *A] Construct design of lentiviral CRISPRv2 vector demonstrating the sgRNA and spCas9 location. B] Nucleotide distribution around the cut site (vertical dashed line) of sgRNA. C] Indel size distribution in untreated samples. D] Mutation position distribution showing the editing profile in untreated samples.*

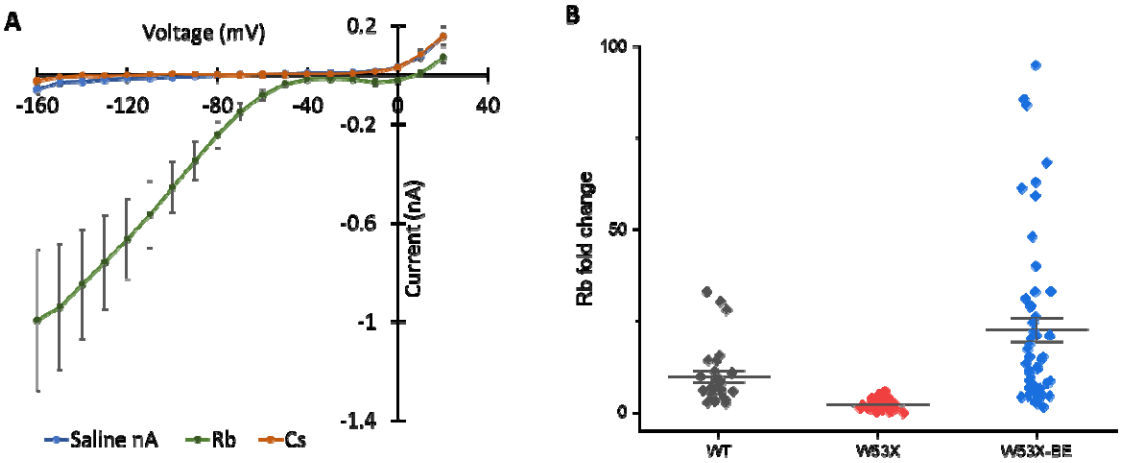

Supplementary Figure 4: Automated patch-clamp recordings from HEK^{W53X}, HEK^{WT,} and $^{HEKW53X\text{-}BE}$ cells. *A] I-V curve for HEK^{WT} cells showing a large negative membrane potential. B] The fold changes for Rb^{+} and Cs^{+} in HEK^{WT}, HEK^{W53X}, and $^{HEKW53X\text{-}BE}$ cells.*

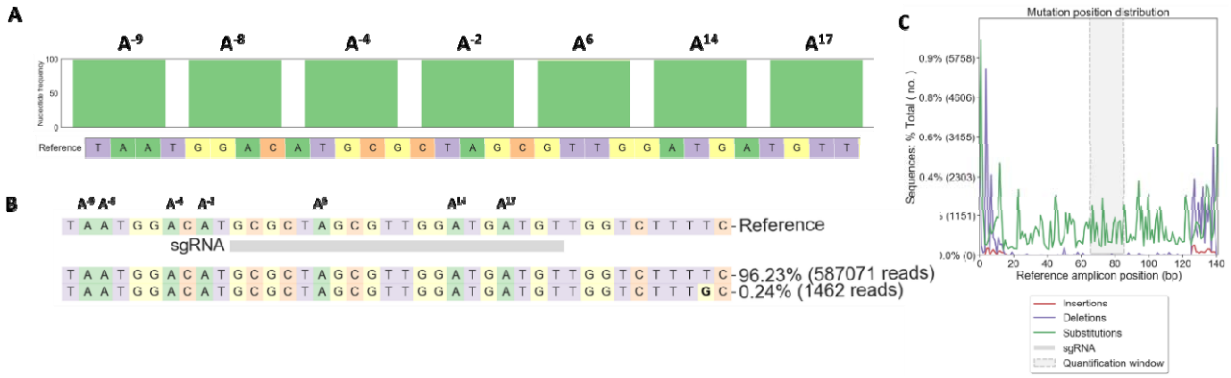

Supplementary Figure 5: Sequencing readouts from untreated LCA16-Fibroblasts^{W53X} used as reference. *A] Nucleotide distribution around sgRNA location as observed in sequencing reads. B] Percentage of sequencing reads observed in the untreated sample. C] Percentage distribution of substitution and deletion at sgRNA location.*

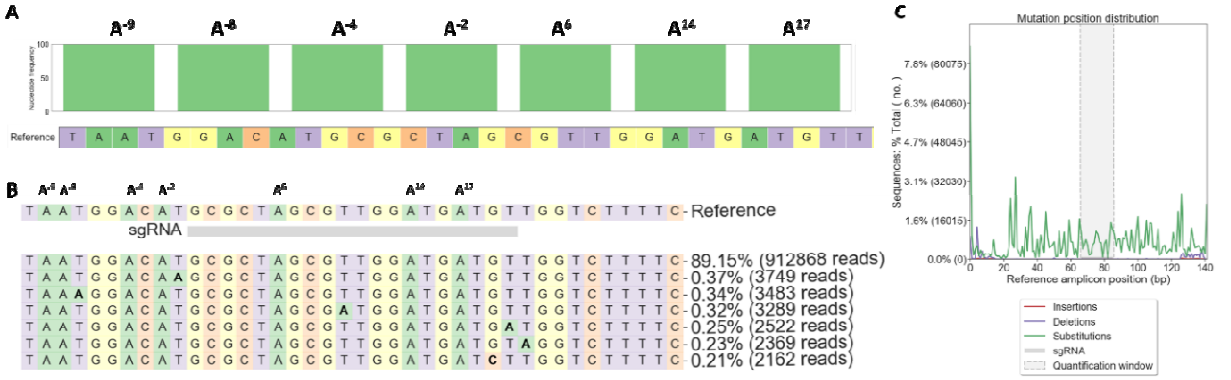

Supplementary Figure 6: Sequencing readouts from untreated iPSC RPE^{W53X} cells used as reference. *A] Nucleotide distribution around sgRNA location as observed in sequencing reads. B] Percentage of sequencing reads observed in the untreated sample. C] Percentage distribution of substitution and deletion at sgRNA location.*

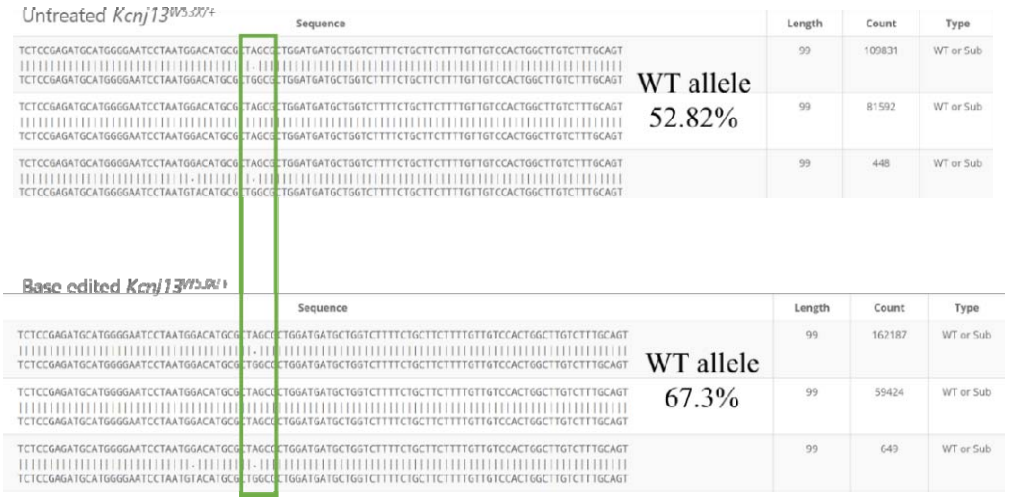

Supplementary Figure 7: Deep sequencing reads from the edited fibroblasts isolated from Kcnj13$^{W53X/-}$ mice. *The sequencing reads were generated by editing mouse W53X alleles within fibroblasts using ABE8e and W53X-sgRNA, delivered via nucleofection.*

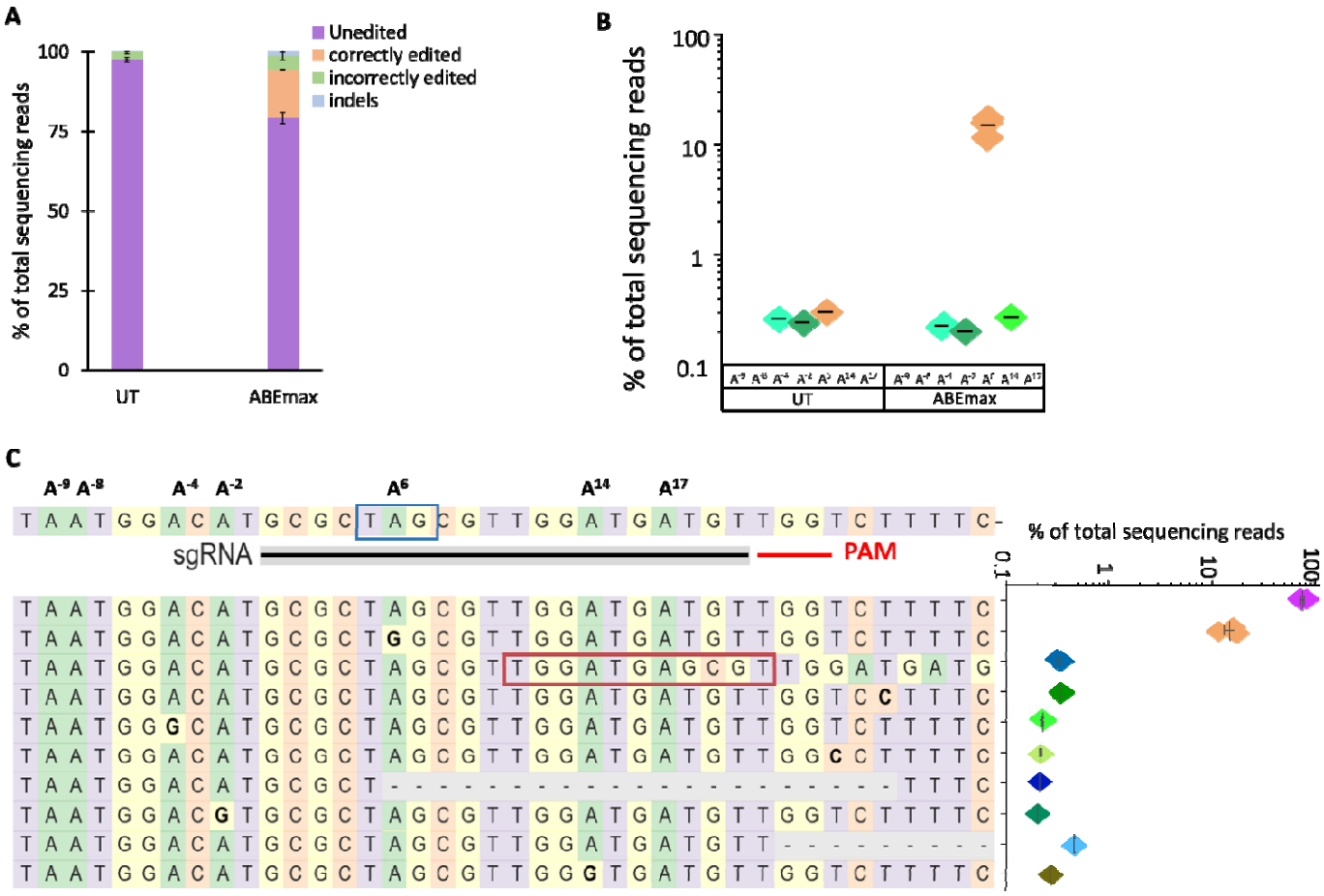

Supplementary Figure 8: Evaluation of ABE7.10max mRNA + sgRNA combinations to correct the W53X allele in Fibro^{W53X}. *A] Base editing efficiencies shown as the % of total DNA sequencing reads, classified as unedited, correctly edited, incorrectly edited due to bystander 'A' edits, and with indels in treated and untreated (UT) cells. B] % Editing of the target (A^{6}) and bystander (A^{-9}, - A^{-8}, A^{-4}, A^{-2}, A^{14}, A^{17}) 'A' to 'G' as observed in three independent experiments. C] The sgRNA location is marked by black line, PAM by red line, and mutation in the blue box. All the 'A' bases within the protospacer are numbered from 1-20 based on their location. The 'A' bases downstream of the protospacer are numbered from -1 to -9, considering +1 as the first base of the protospacer. The top 10 most frequent alleles generated by ABE7.10max mRNA treatment show the nucleotide distribution around the cleavage site for sgRNA. Substitutions are highlighted in bold, insertions are shown in the red box, and deletions are shown by dashes. The scatter plot shows the frequency of reads observed in treated cells (n=3 biological replicates). Figures presenting data from replicates are shown as mean ± SEM.*

References

1. M. Kumar, B. R. Pattnaik, Focus on Kir7.1: physiology and channelopathy. *Channels (Austin)* **8**, 488-495 (2014).
2. M. Kabra, B. R. Pattnaik, Sensing through Non-Sensing Ocular Ion Channels. *Int J Mol Sci* **21**, (2020).
3. W. Zhang, X. Zhang, H. Wang, A. K. Sharma, A. O. Edwards, B. A. Hughes, Characterization of the R162W Kir7.1 mutation associated with snowflake vitreoretinopathy. *Am J Physiol Cell Physiol* **304**, C440-449 (2013).
4. M. Toms, A. M. Dubis, W. S. Lim, A. R. Webster, M. B. Gorin, M. Moosajee, Missense variants in the conserved transmembrane M2 protein domain of KCNJ13 associated with retinovascular changes in humans and zebrafish. *Exp Eye Res* **189**, 107852 (2019).
5. P. I. Sergouniotis, A. E. Davidson, D. S. Mackay, Z. Li, X. Yang, V. Plagnol, A. T. Moore, A. R. Webster, Recessive mutations in KCNJ13, encoding an inwardly rectifying potassium channel subunit, cause leber congenital amaurosis. *Am J Hum Genet* **89**, 183-190 (2011).
6. B. R. Pattnaik, S. Tokarz, M. P. Asuma, T. Schroeder, A. Sharma, J. C. Mitchell, A. O. Edwards, D. A. Pillers, Snowflake vitreoretinal degeneration (SVD) mutation R162W provides new insights into Kir7.1 ion channel structure and function. *PLoS One* **8**, e71744 (2013).
7. B. R. Pattnaik, P. K. Shahi, M. J. Marino, X. Liu, N. York, S. Brar, J. Chiang, D. A. Pillers, E. I. Traboulsi, A Novel KCNJ13 Nonsense Mutation and Loss of Kir7.1 Channel Function Causes Leber Congenital Amaurosis (LCA16). *Hum Mutat* **36**, 720-727 (2015).
8. J. F. Hejtmancik, X. Jiao, A. Li, Y. V. Sergeev, X. Ding, A. K. Sharma, C. C. Chan, I. Medina, A. O. Edwards, Mutations in KCNJ13 cause autosomal-dominant snowflake vitreoretinal degeneration. *Am J Hum Genet* **82**, 174-180 (2008).
9. S. J. Carrington, C. C. Hernandez, D. R. Swale, O. A. Aluko, J. S. Denton, R. D. Cone, G protein-coupled receptors differentially regulate glycosylation and activity of the inwardly rectifying potassium channel Kir7.1. *J Biol Chem* **293**, 17739-17753 (2018).
10. K. M. Beverley, P. K. Shahi, M. Kabra, Q. Zhao, J. Heyrman, J. Steffen, B. R. Pattnaik, Kir7.1 disease mutant T153I within the inner pore affects K+ conduction. *Am J Physiol Cell Physiol*, (2022).
11. P. K. Shahi, D. Hermans, D. Sinha, S. Brar, H. Moulton, S. Stulo, K. D. Borys, E. Capowski, D. M. Pillers, D. M. Gamm, B. R. Pattnaik, Gene Augmentation and Readthrough Rescue Channelopathy in an iPSC-RPE Model of Congenital Blindness. *Am J Hum Genet* **104**, 310-318 (2019).
12. J. Pulman, J. A. Sahel, D. Dalkara, New Editing Tools for Gene Therapy in Inherited Retinal Dystrophies. *CRISPR J* **5**, 377-388 (2022).
13. A. Strong, K. Musunuru, Genome editing in cardiovascular diseases. *Nat Rev Cardiol* **14**, 11-20 (2017).
14. A. Orthwein, S. M. Noordermeer, M. D. Wilson, S. Landry, R. I. Enchev, A. Sherker, M. Munro, J. Pinder, J. Salsman, G. Dellaire, B. Xia, M. Peter, D. Durocher, A mechanism for the suppression of homologous recombination in G1 cells. *Nature* **528**, 422-426 (2015).
15. F. Nami, M. Basiri, L. Satarian, C. Curtiss, H. Baharvand, C. Verfaillie, Strategies for In Vivo Genome Editing in Nondividing Cells. *Trends Biotechnol* **36**, 770-786 (2018).
16. B. R. Webber, C. L. Lonetree, M. G. Kluesner, M. J. Johnson, E. J. Pomeroy, M. D. Diers, W. S. Lahr, G. M. Draper, N. J. Slipek, B. A. Smeester, K. N. Lovendahl, A. N. McElroy, W. R. Gordon, M. J. Osborn, B. S. Moriarity, Highly efficient multiplex human T cell engineering without double-strand breaks using Cas9 base editors. *Nat Commun* **10**, 5222 (2019).

17. J. Tao, Q. Wang, C. Mendez-Dorantes, K. H. Burns, R. Chiarle, Frequency and mechanisms of LINE-1 retrotransposon insertions at CRISPR/Cas9 sites. *Nat Commun* **13**, 3685 (2022).
18. H. Y. Shin, C. Wang, H. K. Lee, K. H. Yoo, X. Zeng, T. Kuhns, C. M. Yang, T. Mohr, C. Liu, L. Hennighausen, CRISPR/Cas9 targeting events cause complex deletions and insertions at 17 sites in the mouse genome. *Nat Commun* **8**, 15464 (2017).
19. G. Schiroli, A. Conti, S. Ferrari, L. Della Volpe, A. Jacob, L. Albano, S. Beretta, A. Calabria, V. Vavassori, P. Gasparini, E. Salataj, D. Ndiaye-Lobry, C. Brombin, J. Chaumeil, E. Montini, I. Merelli, P. Genovese, L. Naldini, R. Di Micco, Precise Gene Editing Preserves Hematopoietic Stem Cell Function following Transient p53-Mediated DNA Damage Response. *Cell Stem Cell* **24**, 551-565 e558 (2019).
20. A. D. Nahmad, E. Reuveni, E. Goldschmidt, T. Tenne, M. Liberman, M. Horovitz-Fried, R. Khosravi, H. Kobo, E. Reinstein, A. Madi, U. Ben-David, A. Barzel, Frequent aneuploidy in primary human T cells after CRISPR-Cas9 cleavage. *Nat Biotechnol*, (2022).
21. M. L. Leibowitz, S. Papathanasiou, P. A. Doerfler, L. J. Blaine, L. Sun, Y. Yao, C. Z. Zhang, M. J. Weiss, D. Pellman, Chromothripsis as an on-target consequence of CRISPR-Cas9 genome editing. *Nat Genet* **53**, 895-905 (2021).
22. R. J. Ihry, K. A. Worringer, M. R. Salick, E. Frias, D. Ho, K. Theriault, S. Kommineni, J. Chen, M. Sondey, C. Ye, R. Randhawa, T. Kulkarni, Z. Yang, G. McAllister, C. Russ, J. Reece-Hoyes, W. Forrester, G. R. Hoffman, R. Dolmetsch, A. Kaykas, p53 inhibits CRISPR-Cas9 engineering in human pluripotent stem cells. *Nat Med* **24**, 939-946 (2018).
23. E. Haapaniemi, S. Botla, J. Persson, B. Schmierer, J. Taipale, CRISPR-Cas9 genome editing induces a p53-mediated DNA damage response. *Nat Med* **24**, 927-930 (2018).
24. O. M. Enache, V. Rendo, M. Abdusamad, D. Lam, D. Davison, S. Pal, N. Currimjee, J. Hess, S. Pantel, A. Nag, A. R. Thorner, J. G. Doench, F. Vazquez, R. Beroukhim, T. R. Golub, U. Ben-David, Cas9 activates the p53 pathway and selects for p53-inactivating mutations. *Nat Genet* **52**, 662-668 (2020).
25. G. Alanis-Lobato, J. Zohren, A. McCarthy, N. M. E. Fogarty, N. Kubikova, E. Hardman, M. Greco, D. Wells, J. M. A. Turner, K. K. Niakan, Frequent loss of heterozygosity in CRISPR-Cas9-edited early human embryos. *Proc Natl Acad Sci U S A* **118**, (2021).
26. A. C. Komor, Y. B. Kim, M. S. Packer, J. A. Zuris, D. R. Liu, Programmable editing of a target base in genomic DNA without double-stranded DNA cleavage. *Nature* **533**, 420-424 (2016).
27. N. M. Gaudelli, A. C. Komor, H. A. Rees, M. S. Packer, A. H. Badran, D. I. Bryson, D. R. Liu, Programmable base editing of A*T to G*C in genomic DNA without DNA cleavage. *Nature* **551**, 464-471 (2017).
28. C. E. Nelson, Y. Wu, M. P. Gemberling, M. L. Oliver, M. A. Waller, J. D. Bohning, J. N. Robinson-Hamm, K. Bulaklak, R. M. Castellanos Rivera, J. H. Collier, A. Asokan, C. A. Gersbach, Long-term evaluation of AAV-CRISPR genome editing for Duchenne muscular dystrophy. *Nat Med* **25**, 427-432 (2019).
29. D. G. Miller, L. M. Petek, D. W. Russell, Adeno-associated virus vectors integrate at chromosome breakage sites. *Nat Genet* **36**, 767-773 (2004).
30. K. S. Hanlon, B. P. Kleinstiver, S. P. Garcia, M. P. Zaborowski, A. Volak, S. E. Spirig, A. Muller, A. A. Sousa, S. Q. Tsai, N. E. Bengtsson, C. Loov, M. Ingelsson, J. S. Chamberlain, D. P. Corey, M. J. Aryee, J. K. Joung, X. O. Breakefield, C. A. Maguire, B. Gyorgy, High levels of AAV vector integration into CRISPR-induced DNA breaks. *Nat Commun* **10**, 4439 (2019).
31. Y. Wang, P. K. Shahi, X. Wang, R. Xie, Y. Zhao, M. Wu, S. Roge, B. R. Pattnaik, S. Gong, In vivo targeted delivery of nucleic acids and CRISPR genome editors enabled by GSH-responsive silica nanoparticles. *J Control Release* **336**, 296-309 (2021).

32. R. Sharma, V. Khristov, A. Rising, B. S. Jha, R. Dejene, N. Hotaling, Y. Li, J. Stoddard, C. Stankewicz, Q. Wan, C. Zhang, M. M. Campos, K. J. Miyagishima, D. McGaughey, R. Villasmil, M. Mattapallil, B. Stanzel, H. Qian, W. Wong, L. Chase, S. Charles, T. McGill, S. Miller, A. Maminishkis, J. Amaral, K. Bharti, Clinical-grade stem cell-derived retinal pigment epithelium patch rescues retinal degeneration in rodents and pigs. *Sci Transl Med* **11**, (2019).
33. G. H. Hwang, J. Park, K. Lim, S. Kim, J. Yu, E. Yu, S. T. Kim, R. Eils, J. S. Kim, S. Bae, Web-based design and analysis tools for CRISPR base editing. *BMC Bioinformatics* **19**, 542 (2018).
34. S. M. Siegner, M. E. Karasu, M. S. Schroder, Z. Kontarakis, J. E. Corn, PnB Designer: a web application to design prime and base editor guide RNAs for animals and plants. *BMC Bioinformatics* **22**, 101 (2021).
35. M. F. Richter, K. T. Zhao, E. Eton, A. Lapinaite, G. A. Newby, B. W. Thuronyi, C. Wilson, L. W. Koblan, J. Zeng, D. E. Bauer, J. A. Doudna, D. R. Liu, Phage-assisted evolution of an adenine base editor with improved Cas domain compatibility and activity. *Nat Biotechnol* **38**, 883-891 (2020).
36. J. Park, K. Lim, J. S. Kim, S. Bae, Cas-analyzer: an online tool for assessing genome editing results using NGS data. *Bioinformatics* **33**, 286-288 (2017).
37. R. H. Clement K, Canver MC, Gehrke JM, Farouni R, Hsu JY, Cole MA, Liu DR, Joung JK, Bauer DE, Pinello L., CRISPResso2 provides accurate and rapid genome editing sequence analysis. *Nat Biotechnol.* **37(3)**, 224-226 (2019).
38. S. Bae, J. Park, J. S. Kim, Cas-OFFinder: a fast and versatile algorithm that searches for potential off-target sites of Cas9 RNA-guided endonucleases. *Bioinformatics* **30**, 1473-1475 (2014).
39. M. Kabra, M. Moosajee, G. A. Newby, K. Molugu, K. Saha, D. R. Liu, B. R. Pattnaik, Comprehensive Analysis of CRISPR Base Editing Outcomes for Multimeric Protein. *bioRxiv*, 2022.2006.2020.496792 (2022).
40. P. K. Shahi, X. Liu, B. Aul, A. Moyer, A. Pattnaik, J. Denton, D. M. Pillers, B. R. Pattnaik, Abnormal Electroretinogram after Kir7.1 Channel Suppression Suggests Role in Retinal Electrophysiology. *Sci Rep* **7**, 10651 (2017).
41. A. Lapinaite, G. J. Knott, C. M. Palumbo, E. Lin-Shiao, M. F. Richter, K. T. Zhao, P. A. Beal, D. R. Liu, J. A. Doudna, DNA capture by a CRISPR-Cas9-guided adenine base editor. *Science* **369**, 566-571 (2020).
42. W. Yin, H. T. Kim, S. Wang, F. Gunawan, L. Wang, K. Kishimoto, H. Zhong, D. Roman, J. Preussner, S. Guenther, V. Graef, C. Buettner, B. Grohmann, M. Looso, M. Morimoto, G. Mardon, S. Offermanns, D. Y. R. Stainier, The potassium channel KCNJ13 is essential for smooth muscle cytoskeletal organization during mouse tracheal tubulogenesis. *Nat Commun* **9**, 2815 (2018).
43. P. D. Stenson, E. V. Ball, M. Mort, A. D. Phillips, J. A. Shiel, N. S. Thomas, S. Abeysinghe, M. Krawczak, D. N. Cooper, Human Gene Mutation Database (HGMD): 2003 update. *Hum Mutat* **21**, 577-581 (2003).
44. M. L. Maeder, M. Stefanidakis, C. J. Wilson, R. Baral, L. A. Barrera, G. S. Bounoutas, D. Bumcrot, H. Chao, D. M. Ciulla, J. A. DaSilva, A. Dass, V. Dhanapal, T. J. Fennell, A. E. Friedland, G. Giannoukos, S. W. Gloskowski, A. Glucksmann, G. M. Gotta, H. Jayaram, S. J. Haskett, B. Hopkins, J. E. Horng, S. Joshi, E. Marco, R. Mepani, D. Reyon, T. Ta, D. G. Tabbaa, S. J. Samuelsson, S. Shen, M. N. Skor, P. Stetkiewicz, T. Wang, C. Yudkoff, V. E. Myer, C. F. Albright, H. Jiang, Development of a gene-editing approach to restore vision loss in Leber congenital amaurosis type 10. *Nat Med* **25**, 229-233 (2019).
45. B. Steyer, Q. Bu, E. Cory, K. Jiang, S. Duong, D. Sinha, S. Steltzer, D. Gamm, Q. Chang, K. Saha, Scarless Genome Editing of Human Pluripotent Stem Cells via Transient Puromycin Selection. *Stem Cell Reports* **10**, 642-654 (2018).